Finite Volume Multigrid for 3D-Problems

P. W. Hemker
CWI
P.O. Box 94079, 1090 GB Amsterdam, The Netherlands

Abstract

We describe a multigrid algorithm for the solution of a three-dimensional second-order elliptic equation. For the approximation of the solution we use a partially ordered hierarchy of finite-volume discretisations. We show that there is a relation with semi-coarsening and approximation by wavelets. A proper subset of all possible meshes in the hierarchy gives rise to a sparse-grid finite-volume discretisation.

The multigrid algorithm consists of a simple damped point-Jacobi relaxation as the smoothing procedure, and a coarse grid correction made by interpolation from several coarser grids levels.

The combination of sparse grids and multigrid with semi-coarsening leads to a relatively small number of degrees of freedom, N, to obtain an accurate approximation, together with an $\mathcal{O}(N)$ method for the solution. The algorithm is symmetric with respect to the three coordinate directions and it is suitable for combination with adaptive techniques.

To analyse the convergence of the multigrid algorithm, we first develop the necessary Fourier analysis tools. All techniques, designed for 3D-problems, can also be applied for the 2D case, and -for simplicity- we apply the tools to study the convergence behaviour for the anisotropic Poisson equation for this 2D case.

Note: Major parts of this paper were already published in [1]).

1 Introduction

We describe the approximation of a function on a hierarchy of finite-volume grids, and a multigrid algorithm for the solution of partial differential equations in three dimensions. The algorithm is developed for the solution of flow problems described by conservation laws, and therefore finite volumes are a natural choice for the discretisation. But to introduce the main principles, we will restrict the treatment here to second order elliptic equations, and in particular to the anisotropic Poisson equation.

In contrast to the usual multigrid approach, we do not use a sequentially ordered set of discretisations on different meshes, but we use a partially ordered hierarchy of 'semi-coarsened' grids as proposed e.g. by Mulder [6, 7] and Naik-VanRosendale [8] or Zenger et al. [3, 9]. As indicated in [9], adaptive 'sparse grid' discretisations can be constructed by taking a suitable subset of all possible discretisations in such a hierarchy. However, in

[1] HEMKER, P.W.: Sparse-Grid Finite-Volume Multigrid for 3D-Problems, *Advances in Comput. Math.*, **4**, 83–110 (1995).

contrast to the sparse grid approximation proposed in [3, 9], we base our approximation on finite volumes rather than on finite elements.

The multigrid algorithm consists of damped Jacobi relaxation as a smoothing procedure and a coarse grid correction constructed by extrapolation from simultaneous corrections on several coarser grids levels.

The algorithm is completely symmetric with respect to the three coordinate directions and it is suitable for combination with adaptive techniques. A description of a data structure to implement such adaptive three-dimensional algorithms is given elsewhere [5].

2 Finite volume sparse grids

In this section we describe finite-volume sparse grids. We show the relation between the approximation by Haar wavelets (when this notion is extended to more dimensions) and the sparse-grid approximation. For the theory of wavelets, multiresolution analysis (MRA) etc. we refer to Daubechies [2].

2.1 A multi-D multiresolution analysis

A *multidimensional multiresolution analysis* of $L^2(\Omega)$, $\Omega = I\!R^3$, is a partially ordered set of closed linear subspaces

$$\{V_{\boldsymbol{n}} | V_{\boldsymbol{n}} \subset L^2(\Omega)\}_{\boldsymbol{n}\in Z\!\!Z^3}$$

with the properties:

$$\begin{array}{ll} (1) & \cap_{\boldsymbol{n}} V_{\boldsymbol{n}} = \{0\}; \quad \cup_{\boldsymbol{n}} V_{\boldsymbol{n}} \subset_{\text{dense}} L^2(\Omega); \\ (2) & f(\boldsymbol{x})\in V_{\boldsymbol{n}} \Leftrightarrow f(2^{\boldsymbol{m}}\boldsymbol{x})\in V_{\boldsymbol{n}+\boldsymbol{m}} \quad \forall \boldsymbol{n}\in Z\!\!Z^3, \boldsymbol{m}\in \mathbf{E}; \\ (3) & f(\boldsymbol{x})\in V_{\boldsymbol{n}} \Leftrightarrow f(\boldsymbol{x}-2^{-\boldsymbol{n}}\boldsymbol{k})\in V_{\boldsymbol{n}} \quad \forall \boldsymbol{k}\in Z\!\!Z^3, \boldsymbol{n}\in \mathbf{E}; \\ (4) & \exists \phi\in V_{\mathbf{o}} : \ \{\phi(\boldsymbol{x}-\boldsymbol{k})\}_{\boldsymbol{k}\in Z\!\!Z^3} \text{ is a Riesz basis for } V_{\mathbf{o}}. \end{array} \tag{1}$$

Here $\boldsymbol{n} = (n_1, n_2, n_3)\in Z\!\!Z^3$, and we denote $|\boldsymbol{n}| = n_1 + n_2 + n_3$; $2^{\boldsymbol{n}} = (2^{n_1}, 2^{n_2}, 2^{n_3})$. We also use the notation $\mathbf{o} = (0,0,0)\in I\!N^3$; $\boldsymbol{x} = (x_1, x_2, x_3)\in I\!R^3$; $2^{\boldsymbol{n}}\boldsymbol{x} = (2^{n_1}x_1, 2^{n_2}x_2, 2^{n_3}x_3)$. Further we introduce in $I\!N^3$ the unit vectors $\boldsymbol{e}_k$, $k = 1,2,3$, as follows: $\boldsymbol{e}_1 = (1,0,0)$; $\boldsymbol{e}_2 = (0,1,0)$; $\boldsymbol{e}_3 = (0,0,1)$, and we use $\boldsymbol{e} = (1,1,1)$. Finally we define $\mathbf{E} = \{\boldsymbol{e}_1, \boldsymbol{e}_2, \boldsymbol{e}_3\}$. Although we are particularly interested in the three-dimensional case, generalisation to a different number of space dimensions is straightforward. The function $\phi(\boldsymbol{x})$ in (1.4) is called the the *scaling function* of the multiresolution analysis.

2.2 Piecewise constant function spaces

Let either $\Omega = I\!R^3$ be the three-dimensional Euclidean space, or let $\Omega = (0,1)^3 \subset I\!R^3$ be the open unit cube. For any $\boldsymbol{n}\in Z\!\!Z^3$ we introduce the function space $V_{\boldsymbol{n}}$, i.e. the space of piecewise constant functions on a uniform grid with meshsize $\boldsymbol{h} = (2^{-n_1}, 2^{-n_2}, 2^{-n_3})$. These grids are uniformly spaced in each of the three coordinate directions, but possibly with a different meshsize in the different directions. The volume of these cells is denoted by $h^3 = 2^{-|\boldsymbol{n}|}$. The functions in $V_{\boldsymbol{n}}$ are all constant in each *cell*

$$\Omega_{\boldsymbol{n},\boldsymbol{k}} = [k_1 2^{-n_1}, (k_1+1)2^{-n_1}] \times [k_2 2^{-n_2}, (k_2+1)2^{-n_2}] \times [k_3 2^{-n_3}, (k_3+1)2^{-n_3}],$$

and this family of cells forms the *grid* $\Omega_{\boldsymbol{n}} = \{\Omega_{\boldsymbol{n},\boldsymbol{k}} \mid \Omega_{\boldsymbol{n},\boldsymbol{k}} \subset \Omega, \boldsymbol{k} \in \mathbb{Z}^3\}$. The family of *cell nodes* is denoted by $\Omega^*_{\boldsymbol{n}} = \{z_{\boldsymbol{n},\boldsymbol{k}} \mid z_{\boldsymbol{n},\boldsymbol{k}} = (\boldsymbol{k} + \boldsymbol{e}/2)2^{-\boldsymbol{n}};\ \boldsymbol{k} \in \mathbb{Z}^3;\ z_{\boldsymbol{n},\boldsymbol{k}} \in \overline{\Omega}\}$. The number of these nodes is equal to the dimension of $V_{\boldsymbol{n}}$.

Apparently, all grids are identified by a triple $\boldsymbol{n}$; the number $|\boldsymbol{n}|$ is called the *level* of the grid $\boldsymbol{n}$. Notice that –different from classical multigrid– here and later in our multigrid algorithm, there is a clear distinction between the grid-identification index $\boldsymbol{n}$ and the level number $|\boldsymbol{n}|$.

We define the relational operators ($\leq, <, =, >, \geq$ etc.) between triples by

$$\boldsymbol{n} \leq \boldsymbol{m} \Leftrightarrow n_1 \leq m_1,\ n_2 \leq m_2,\ n_3 \leq m_3\,.$$

Because

$$V_{\boldsymbol{n}} \subset V_{\boldsymbol{n}+\boldsymbol{e}_j}\,, \qquad \text{for } j = 1, 2, 3, \tag{2}$$

we see, by construction, that nesting relations exist between spaces $V_{\boldsymbol{n}}$ and that the nesting provides a partial ordering:

$$V_{\boldsymbol{n}} \subset V_{\boldsymbol{m}} \Leftrightarrow \boldsymbol{n} \leq \boldsymbol{m}. \tag{3}$$

Spaces $V_{\boldsymbol{n}}$ and $V_{\boldsymbol{m}}$ or grids $\Omega_{\boldsymbol{n}}$ and $\Omega_{\boldsymbol{m}}$ that satisfy this nesting relation $\boldsymbol{n} < \boldsymbol{m}$ are called *related*. The construction of the spaces $V_{\boldsymbol{n}}$ shows that even a stronger relation holds than (2), namely

$$V_{\boldsymbol{n}-\boldsymbol{e}_j} \cap V_{\boldsymbol{n}-\boldsymbol{e}_k} = V_{\boldsymbol{n}-\boldsymbol{e}_j-\boldsymbol{e}_k}\,, \qquad j, k = 1, 2, 3,\ \ j \neq k. \tag{4}$$

We see also that for $\Omega = \mathbb{R}^3$ the spaces $\{V_{\boldsymbol{n}}\}_{\boldsymbol{n} \in \mathbb{Z}^3}$ form a multiresolution analysis and that in this case the characteristic function on the unit cube, $\phi \in V_{\mathbf{0}}$,

$$\phi(\boldsymbol{x}) = \begin{cases} 1 & \text{if } \ x \in \Omega_{\mathbf{0},\mathbf{0}}, \\ 0 & \text{if } \ x \notin \Omega_{\mathbf{0},\mathbf{0}}, \end{cases} \tag{5}$$

serves as the scaling function. The set $\{\phi^{\boldsymbol{n}}_{\boldsymbol{k}} \mid \phi^{\boldsymbol{n}}_{\boldsymbol{k}}(\boldsymbol{x}) = \phi(2^{\boldsymbol{n}}\boldsymbol{x} - \boldsymbol{k}), \boldsymbol{k} \in \mathbb{Z}^3\}$ forms a basis in $V_{\boldsymbol{n}}$, which corresponds with the usual Haar-basis for the one-dimensional case.

In the case $\Omega = (0,1)^3$ we restrict ourselves to $V_{\boldsymbol{n}}$ with $n_1, n_2, n_3 \geq 0$ and we see $\dim(V_{\boldsymbol{n}}) = 2^{|\boldsymbol{n}|}$. Formally, for $\Omega = (0,1)^3$ and n_1, n_2 or n_3 negative we define $V_{\boldsymbol{n}} = V_{n_1,n_2,n_3}$ by $V_{\boldsymbol{n}} = \{0\}$.

For all spaces $V_{\boldsymbol{n}}$ we introduce the restriction operator $R_{\boldsymbol{n}} : L^2(\Omega) \to V_{\boldsymbol{n}}$, the L^2-projection such that for $u \in L^2(\Omega)$ we have $R_{\boldsymbol{n}}u \in V_{\boldsymbol{n}}$ and

$$(R_{\boldsymbol{n}}u)(z_{\boldsymbol{n},\boldsymbol{k}}) = 2^{|\boldsymbol{n}|} \int_{\Omega_{\boldsymbol{n},\boldsymbol{k}}} u(z)\, dz\,. \tag{6}$$

2.3 More-dimensional wavelets

We introduce the wavelet space $W_{\boldsymbol{n}} \subset V_{\boldsymbol{n}}$ which consists of all functions in $V_{\boldsymbol{n}}$ that are not represented in any of the related function spaces on the next coarser level, i.e. they are in $V_{\boldsymbol{n}}$ but not in $\mathrm{Span}(V_{\boldsymbol{n}-\boldsymbol{e}_1}, V_{\boldsymbol{n}-\boldsymbol{e}_2}, V_{\boldsymbol{n}-\boldsymbol{e}_3})$, or

$$V_{\boldsymbol{n}} = W_{\boldsymbol{n}} \ \oplus\ \mathrm{Span}(V_{\boldsymbol{n}-\boldsymbol{e}_1}, V_{\boldsymbol{n}-\boldsymbol{e}_2}, V_{\boldsymbol{n}-\boldsymbol{e}_3}), \tag{7}$$

This means that $W_{\boldsymbol{n}}$ contains the 'difference information' that is available in the fine grid $V_{\boldsymbol{n}}$ but not in the the span of the coarser grids $V_{\boldsymbol{n}-\boldsymbol{e}_1}$, $V_{\boldsymbol{n}-\boldsymbol{e}_2}$ and $V_{\boldsymbol{n}-\boldsymbol{e}_3}$.

In our case, where $V_{\boldsymbol{n}}$ contains the piecewise constant functions, it is simple to construct the spaces $W_{\boldsymbol{n}}$ such that

$$W_{\boldsymbol{n}} \perp \mathrm{Span}(V_{\boldsymbol{n}-\boldsymbol{e}_1}, V_{\boldsymbol{n}-\boldsymbol{e}_2}, V_{\boldsymbol{n}-\boldsymbol{e}_3}). \tag{8}$$

This makes $W_{\boldsymbol{n}}$ the orthogonal complement of $\mathrm{Span}(V_{\boldsymbol{n}-(1,0,0)}, V_{\boldsymbol{n}-(0,1,0)}, V_{\boldsymbol{n}-(0,0,1)})$ in $V_{\boldsymbol{n}}$.

For $\Omega \subset I\!R^3$ the relation (8) allows a straightforward decomposition of $V_{\boldsymbol{n}}$. In the case $\Omega = I\!R^3$ we have

$$V_{\boldsymbol{n}}(I\!R^3) = \bigoplus_{j_1=-\infty}^{n_1} \bigoplus_{j_2=-\infty}^{n_2} \bigoplus_{j_3=-\infty}^{n_3} W_{\boldsymbol{j}}, \tag{9}$$

where all $W_{\boldsymbol{j}}$ are orthogonal to each other. Notice that here, in the more-dimensional case, it is convenient to choose an indexing that is different from the usual indexing in the well-known one-dimensional case.

To handle the bounded domain $\Omega = (0,1)^3$ we introduce the functions $V^0_{\boldsymbol{n}}(\Omega) \subset V_{\boldsymbol{n}}(\Omega)$ which have a zero mean value on Ω, i.e. $V^0_{\boldsymbol{n}}(\Omega) = \{u \in V_{\boldsymbol{n}}(\Omega) \mid R_{\mathbf{0}}(u) = 0\}$, and we have

$$V^0_{\boldsymbol{n}}(\Omega) = \bigoplus_{j_1=0}^{n_1} \bigoplus_{j_2=0}^{n_2} \bigoplus_{j_3=0}^{n_3} W_{\boldsymbol{j}}\,, \tag{10}$$

and hence

$$V_{\boldsymbol{n}}(\Omega) = V_{\mathbf{0}} \oplus V^0_{\boldsymbol{n}} = V_{\mathbf{0}} \oplus \bigoplus_{\mathbf{0} \le \boldsymbol{j} \le \boldsymbol{n}} W_{\boldsymbol{j}}\,. \tag{11}$$

The 'difference information' between the approximations of a function $f \in L^2(\Omega)$ on two successive levels, $R_{\boldsymbol{n}} f \in V_{\boldsymbol{n}}$ on the one hand and $R_{\boldsymbol{n}-\boldsymbol{e}_j} f \in V_{\boldsymbol{n}-\boldsymbol{e}_j}$, $j = 1,2,3$, on the other hand, is given by the orthogonal projection $Q_{\boldsymbol{n}} f$ of f onto the orthogonal complement $W_{\boldsymbol{n}}$ of $V_{\boldsymbol{n}-\boldsymbol{e}_j}$ in $V_{\boldsymbol{n}}$. This is described in the following theorem.

Theorem 2.1 Let the operator $Q_{\boldsymbol{n}} : L^2(\Omega) \to W_{\boldsymbol{n}}$ be the orthogonal projection onto $W_{\boldsymbol{n}}$, then it follows that

$$\begin{aligned} Q_{\boldsymbol{n}} u = R_{\boldsymbol{n}} u \;&- R_{\boldsymbol{n}-\boldsymbol{e}_1} u - R_{\boldsymbol{n}-\boldsymbol{e}_2} u - R_{\boldsymbol{n}-\boldsymbol{e}_3} u \\ &+ R_{\boldsymbol{n}-\boldsymbol{e}_2-\boldsymbol{e}_3} u + R_{\boldsymbol{n}-\boldsymbol{e}_1-\boldsymbol{e}_3} u + R_{\boldsymbol{n}-\boldsymbol{e}_1-\boldsymbol{e}_2} u - R_{\boldsymbol{n}-\boldsymbol{e}} u\,, \end{aligned}$$

or, equivalently,

$$Q_{\boldsymbol{n}} u = R_{\boldsymbol{n}} u - R_{\boldsymbol{n}-\boldsymbol{e}} u + \sum_{j=1,2,3} \left(R_{\boldsymbol{n}-\boldsymbol{e}+\boldsymbol{e}_j} u - R_{\boldsymbol{n}-\boldsymbol{e}_j} u \right). \tag{12}$$

Proof: From (9) or (11) it follows that (possibly neglecting functions in $V_{\mathbf{0}}$ if Ω is the open unit cube) $V_{\boldsymbol{n}} = \oplus_{\boldsymbol{j} \le \boldsymbol{n}} W_{\boldsymbol{j}}$, so that $R_{\boldsymbol{n}} u = \sum_{\boldsymbol{j} \le \boldsymbol{n}} Q_{\boldsymbol{j}} u$, and

$$\begin{aligned} & R_{\boldsymbol{n}} - R_{\boldsymbol{n}-\boldsymbol{e}_1} - R_{\boldsymbol{n}-\boldsymbol{e}_2} - R_{\boldsymbol{n}-\boldsymbol{e}_3} \\ & + R_{\boldsymbol{n}-\boldsymbol{e}_2-\boldsymbol{e}_3} + R_{\boldsymbol{n}-\boldsymbol{e}_1-\boldsymbol{e}_3} + R_{\boldsymbol{n}-\boldsymbol{e}_1-\boldsymbol{e}_2} - R_{\boldsymbol{n}-\boldsymbol{e}} \\ = \;& \textstyle\sum_{\boldsymbol{j} \le \boldsymbol{n}} Q_{\boldsymbol{j}} - \sum_{\boldsymbol{j} \le \boldsymbol{n}-\boldsymbol{e}_1} Q_{\boldsymbol{j}} - \sum_{\boldsymbol{j} \le \boldsymbol{n}-\boldsymbol{e}_2} Q_{\boldsymbol{j}} - \sum_{\boldsymbol{j} \le \boldsymbol{n}-\boldsymbol{e}_3} Q_{\boldsymbol{j}} \\ & + \textstyle\sum_{\boldsymbol{j} \le \boldsymbol{n}-\boldsymbol{e}_2-\boldsymbol{e}_3} Q_{\boldsymbol{j}} + \sum_{\boldsymbol{j} \le \boldsymbol{n}-\boldsymbol{e}_1-\boldsymbol{e}_3} Q_{\boldsymbol{j}} + \sum_{\boldsymbol{j} \le \boldsymbol{n}-\boldsymbol{e}_1-\boldsymbol{e}_2} Q_{\boldsymbol{j}} - \sum_{\boldsymbol{j} \le \boldsymbol{n}-\boldsymbol{e}} Q_{\boldsymbol{j}} \\ = \;& \textstyle\sum_{\boldsymbol{n}-\boldsymbol{e} < \boldsymbol{j} \le \boldsymbol{n}} Q_{\boldsymbol{j}} + \sum_{\boldsymbol{n}-\boldsymbol{e}_1 < \boldsymbol{j} \le \boldsymbol{n}} Q_{\boldsymbol{j}} + \sum_{\boldsymbol{n}-\boldsymbol{e}_2 < \boldsymbol{j} \le \boldsymbol{n}} Q_{\boldsymbol{j}} + \sum_{\boldsymbol{n}-\boldsymbol{e}_3 < \boldsymbol{j} \le \boldsymbol{n}} Q_{\boldsymbol{j}} \\ & - \textstyle\sum_{\boldsymbol{n}-\boldsymbol{e}_2-\boldsymbol{e}_3 < \boldsymbol{j} \le \boldsymbol{n}} Q_{\boldsymbol{j}} - \sum_{\boldsymbol{n}-\boldsymbol{e}_1-\boldsymbol{e}_3 < \boldsymbol{j} \le \boldsymbol{n}} Q_{\boldsymbol{j}} - \sum_{\boldsymbol{n}-\boldsymbol{e}_1-\boldsymbol{e}_2 < \boldsymbol{j} \le \boldsymbol{n}} Q_{\boldsymbol{j}} \\ = \;& Q_{\boldsymbol{n}}\,. \end{aligned}$$

□

Remarks:

- In the right-hand-side of equation (12) we recognise the information that can be represented on the levels $|\boldsymbol{n}|$, $|\boldsymbol{n}|-3$, $|\boldsymbol{n}|-2$, $|\boldsymbol{n}|-1$, respectively.
- In (12) the information on the level $|\boldsymbol{n}|-2$ and $|\boldsymbol{n}|-3$ can directly be derived from the information on level $|\boldsymbol{n}|-1$, e.g. by $R_{\boldsymbol{n}-\boldsymbol{e}_2-\boldsymbol{e}_3}u = R_{\boldsymbol{n}-\boldsymbol{e}_2-\boldsymbol{e}_3}(R_{\boldsymbol{n}-\boldsymbol{e}_3}u)$. Thus, expression (12) describes the difference information between $R_{\boldsymbol{n}}u$ and its approximation on the related next coarser grids.
- Notice that in the two-dimensional case the relation (12) reduces to

$$Q_{\boldsymbol{n}}u = R_{\boldsymbol{n}}u - R_{\boldsymbol{n}-\boldsymbol{e}_1}u - R_{\boldsymbol{n}-\boldsymbol{e}_2}u + R_{\boldsymbol{n}-\boldsymbol{e}}u\,, \tag{13}$$

  where $\boldsymbol{e} = (1,1)$, and in the one-dimensional case we have

$$Q_{\boldsymbol{n}}u = R_{\boldsymbol{n}}u - R_{\boldsymbol{n}-\boldsymbol{e}}u\,. \tag{14}$$

First, in the remainder of this section we restrict ourselves to the case of the unbounded domain $\Omega = \mathbb{R}^3$. The four relations (1.1) to (1.4) imply that also the spaces $W_{\boldsymbol{n}}$ are scaled versions of one space $W_{\boldsymbol{0}}$,

$$f(\boldsymbol{x})\in W_{\boldsymbol{n}} \Leftrightarrow f(2^{-\boldsymbol{n}}\boldsymbol{x})\in W_{\boldsymbol{0}}, \quad \forall \boldsymbol{n}\in\mathbb{Z}^3\,, \tag{15}$$

and, moreover, that they are translation invariant for the discrete translations $2^{-\boldsymbol{n}}\mathbb{Z}^3$,

$$f(\boldsymbol{x})\in W_{\boldsymbol{0}} \Leftrightarrow f(\boldsymbol{x}-\boldsymbol{k})\in W_{\boldsymbol{0}}, \quad \forall \boldsymbol{n}\in\mathbb{Z}^3\,. \tag{16}$$

The relations (7) and (8) make that they are mutually orthogonal spaces, generating all functions of $L^2(\mathbb{R}^3)$,

$$\begin{array}{l} W_{\boldsymbol{n}} \perp W_{\boldsymbol{m}} \quad \text{for } \boldsymbol{n}\neq\boldsymbol{m}, \\ \oplus_{\boldsymbol{n}\in\mathbb{Z}^3} W_{\boldsymbol{n}} \subset_{\text{dense}} L^2(\mathbb{R}^3). \end{array} \tag{17}$$

As soon as we find a function $\psi(\boldsymbol{x})$ with the property that $\psi(\boldsymbol{x}-\boldsymbol{k})$, $k\in\mathbb{Z}^3$, is a basis of $W_{\boldsymbol{e}}$, then by a simple rescaling, we see that $\psi(2^{\boldsymbol{n}}\boldsymbol{x}-\boldsymbol{k})$, yields a basis of $W_{\boldsymbol{n}+\boldsymbol{e}}$. Such a function is the more-dimensional generalisation of a wavelet. Since $L^2(\mathbb{R}^3)$ is the direct sum of these $W_{\boldsymbol{n}+\boldsymbol{e}}$, the full collection $\left\{\psi_{\boldsymbol{k}}^{\boldsymbol{n}+\boldsymbol{e}}(\boldsymbol{x}) \mid \psi_{\boldsymbol{k}}^{\boldsymbol{n}+\boldsymbol{e}}(\boldsymbol{x}) = \psi(2^{\boldsymbol{n}}\boldsymbol{x}-\boldsymbol{k}),\ \boldsymbol{n},\boldsymbol{k}\in\mathbb{Z}^3\right\}$ is a basis of $L^2(\mathbb{R}^3)$.

It is easy to check that the more-dimensional wavelet $\psi(\boldsymbol{x})\in W_{\boldsymbol{e}}$, corresponding with the scaling function $\phi(\boldsymbol{x})\in V_{\boldsymbol{0}}$, from the previous section, is the three-dimensional checkerboard basis function given by (5):

$$\psi(\boldsymbol{x}) = \begin{cases} = & 0 & \text{if } \boldsymbol{x}\notin\Omega_{\boldsymbol{0},\boldsymbol{0}}\,, \\ = & +1 & \text{if } \boldsymbol{x}\in\Omega_{\boldsymbol{0},\boldsymbol{0}}\,, \quad \boldsymbol{x}\in\Omega_{\boldsymbol{e},\boldsymbol{k}}\,, \quad |\boldsymbol{k}| \text{ even}, \\ = & -1 & \text{if } \boldsymbol{x}\in\Omega_{\boldsymbol{0},\boldsymbol{0}}\,, \quad \boldsymbol{x}\in\Omega_{\boldsymbol{e},\boldsymbol{k}}\,, \quad |\boldsymbol{k}| \text{ odd}. \end{cases}$$

This function is the three-dimensional generalisation of the Haar-wavelet. Notice $\psi\in W_{\boldsymbol{e}} \subset V_{\boldsymbol{e}}$ is a function piecewise constant on $\Omega_{\boldsymbol{e}}$.

In wavelet theory the spaces $W_{\boldsymbol{n}}$ are labelled *channels*, and the distinct channels are linearly independent. The first decomposition of an arbitrary function from $L^2(\Omega)$

with $\Omega = I\!R^3$ consists in writing $u(\boldsymbol{x}) = \sum_{\boldsymbol{n}} u_{\boldsymbol{n}}(\boldsymbol{x})$, where each $u_{\boldsymbol{n}}$ belongs to the corresponding channel $W_{\boldsymbol{n}}$ with $\boldsymbol{n} \in \mathbb{Z}^3$.

Similarly, we can write for functions defined on $\Omega = (0,1)^3$ the relation (11) and make a similar decomposition in channels. Each subspace $W_{\boldsymbol{n}+\boldsymbol{e}}$, $\boldsymbol{n} \geq \mathbf{o}$, has its natural basis, the *standard basis*

$$\left\{\psi_{\boldsymbol{k}}^{\boldsymbol{n}+\boldsymbol{e}}(\boldsymbol{x}) \mid \psi_{\boldsymbol{k}}^{\boldsymbol{n}+\boldsymbol{e}}(\boldsymbol{x}) = \psi(2^{\boldsymbol{n}}\boldsymbol{x} - \boldsymbol{k})\right\}$$

of functions with a minimal support. The basis function $\psi_{\boldsymbol{k}}^{\boldsymbol{n}+\boldsymbol{e}}$ is a scaled, elementary checkerboard function, that may be characterised either by its support which is a single cell in $\Omega_{\boldsymbol{n}}$ or by the centerpoint of this cell, $\boldsymbol{z}_{\boldsymbol{n},\boldsymbol{k}}$.

For $\Omega = (0,1)^3$, the exceptions related with the boundary are found in the spaces $W_{\boldsymbol{n}}$ with a zero index (i.e. $n_1 \cdot n_2 \cdot n_3 = 0$). These $W_{\boldsymbol{n}}$ have basis functions with different shapes. They are derived from the corresponding functions for the unbounded case, but their support is restricted to $\Omega_{\boldsymbol{n}-\boldsymbol{e}} \cap \Omega$. Their corresponding nodal points $\boldsymbol{z}_{\boldsymbol{n}-\boldsymbol{e},\boldsymbol{k}}$ are found on the boundary $\partial\Omega = \overline{\Omega}\backslash\Omega$, $\boldsymbol{n} \leq \boldsymbol{e}$, $\boldsymbol{n} \neq \mathbf{o}$. Taking this into account, both for $\Omega = (0,1)^3$ and for $\Omega = I\!R$ we may write for each $u \in L^2(\Omega)$ a wavelet expansion

$$u(\boldsymbol{x}) = \sum_{\boldsymbol{n},\boldsymbol{k}} a_{\boldsymbol{n},\boldsymbol{k}}\, \psi(2^{\boldsymbol{n}}\boldsymbol{x} - \boldsymbol{k}). \tag{18}$$

2.4 Approximation results

The decompositions (9) or (11) clearly allow the approximation of a sufficiently smooth function in $L^2(\Omega)$ by a series with elements in $W_{\boldsymbol{j}}$. To obtain an impression of the quality of these expansions we derive some error estimates.

As the case where boundaries are present is the more general one, we take $\Omega = (0,1)^3$. To quantify the error of approximation on Ω, we introduce for $u \in C^3(\overline{\Omega})$ the seminorm

$$|u| = \sup_{\boldsymbol{x}\in\Omega} \left| \frac{\partial^3 u(\boldsymbol{x})}{\partial x_1 \partial x_2 \partial x_3} \right| + \tag{19}$$

$$\max_{p,q,r=0,1} \sup_{\boldsymbol{x}\in\partial\Omega} \left| \left(\frac{\partial}{\partial x_1}\right)^p \left(\frac{\partial}{\partial x_2}\right)^q \left(\frac{\partial}{\partial x_3}\right)^r u(\boldsymbol{x}) \right| .$$

Now we derive the following

Theorem 2.2 If we consider an expansion of a $C^3(\overline{\Omega})$-function, u, in piecewise constant functions on the grid $\Omega_{\boldsymbol{n}}$, for an arbitrary $\boldsymbol{n} \in \mathbb{Z}^3$, $\boldsymbol{n} > \mathbf{o}$, and if we write

$$R_{\boldsymbol{n}} u = v_{\mathbf{o}} + \sum_{\mathbf{o} \leq \boldsymbol{j} \leq \boldsymbol{n}} u_{\boldsymbol{j}}\,, \tag{20}$$

with $v_{\mathbf{o}} \in V_{\mathbf{o}}$ and $u_{\boldsymbol{j}} \in W_{\boldsymbol{j}}$, $\mathbf{o} \leq \boldsymbol{j} \leq \boldsymbol{n}$, then

$$\|u_{\boldsymbol{j}}\| \leq 2^{|\boldsymbol{j}|}\, |u|\,, \tag{21}$$

and we get an estimate for the approximation error

$$\|u - R_{\boldsymbol{n}} u\| \leq \frac{1}{3}\sqrt{\frac{2}{3}}\,(h_1 + h_2 + h_3)\, |u|\,. \tag{22}$$

Proof: We take the normalised $\{\tilde{\psi}_{\boldsymbol{j}}^{\boldsymbol{k}}\} = \{2^{|\boldsymbol{j}-\boldsymbol{e}|/2}\psi_{\boldsymbol{k}}^{\boldsymbol{j}}\}$ as a basis in $W_{\boldsymbol{j}}$, $\mathbf{o} \le \boldsymbol{j} \le \boldsymbol{n}$, $\boldsymbol{j} \neq \mathbf{o}$. Clearly, all these functions are orthogonal to all functions $v_{\mathbf{o}} \in V_{\mathbf{o}}$ and mutually they form an orthonormal set in $W_{\boldsymbol{j}} \subset L^2(\Omega)$. We see further $\psi_{\boldsymbol{k}}^{\boldsymbol{j}} \in W_{\boldsymbol{j}}$ and $\text{support}(\psi_{\boldsymbol{k}}^{\boldsymbol{j}}) = \Omega_{\boldsymbol{j}-\boldsymbol{e},\boldsymbol{k}}$, or, in other words, $\psi_{\boldsymbol{k}}^{\boldsymbol{j}} \in V_{\boldsymbol{j}}$, but $\psi_{\boldsymbol{k}}^{\boldsymbol{j}}$ scales like a basis function in $V_{\boldsymbol{j}-\boldsymbol{e}}$. Hence

$$\int 2^{|\boldsymbol{j}-\boldsymbol{e}|/2}\psi_{\boldsymbol{k}}^{\boldsymbol{j}}\, 2^{|\boldsymbol{j}-\boldsymbol{e}|/2}\psi_{\boldsymbol{m}}^{\boldsymbol{j}}\, d\Omega = 0 \quad \text{for} \quad \boldsymbol{k} \neq \boldsymbol{m},$$

and

$$\int 2^{|\boldsymbol{j}-\boldsymbol{e}|/2}\psi_{\boldsymbol{k}}^{\boldsymbol{j}}\, 2^{|\boldsymbol{j}-\boldsymbol{e}|/2}\psi_{\boldsymbol{k}}^{\boldsymbol{j}}\, d\Omega = 2^{|\boldsymbol{j}-\boldsymbol{e}|}\int_{\Omega_{\boldsymbol{j}-\boldsymbol{e},\boldsymbol{k}}} d\Omega = 1.$$

Thus, we find (20) with

$$u_{\boldsymbol{j}} = \sum_{\boldsymbol{k}} a_{\boldsymbol{j}\boldsymbol{k}}\,\tilde{\psi}_{\boldsymbol{k}}^{\boldsymbol{j}} = \sum_{\boldsymbol{k}} (u, \tilde{\psi}_{\boldsymbol{k}}^{\boldsymbol{j}})\tilde{\psi}_{\boldsymbol{k}}^{\boldsymbol{j}}.$$

Now

$$a_{\boldsymbol{j}\boldsymbol{k}} = (u, \tilde{\psi}_{\boldsymbol{k}}^{\boldsymbol{j}}) = \int_{\Omega} u\,\tilde{\psi}_{\boldsymbol{k}}^{\boldsymbol{j}}\, d\Omega = \int_{\Omega_{\boldsymbol{j}-\boldsymbol{e},\boldsymbol{k}}} u\,\tilde{\psi}_{\boldsymbol{k}}^{\boldsymbol{j}}\, d\Omega.$$

By Taylor expansion around $\boldsymbol{z}_{\boldsymbol{k}}^{\boldsymbol{j}-\boldsymbol{e}}$, we have

$$\left| \int_{\Omega_{\boldsymbol{j}-\boldsymbol{e},\boldsymbol{k}}} u\,\tilde{\psi}_{\boldsymbol{k}}^{\boldsymbol{j}}\, d\Omega \right| \le 2^{-2|\boldsymbol{j}|}\, 2^{|\boldsymbol{j}-\boldsymbol{e}|/2}\, |u|. \tag{23}$$

For $\boldsymbol{j} \ge \boldsymbol{e}$ the point $\boldsymbol{z}_{\boldsymbol{k}}^{\boldsymbol{j}-\boldsymbol{e}}$ lies in the interior of Ω and the estimate holds with

$$|u| = \max \left| \frac{\partial^3 u(\boldsymbol{x})}{\partial x_1 \cdots \partial x_3} \right|.$$

For $\psi_{\boldsymbol{k}}^{\boldsymbol{j}}$ with a $\boldsymbol{j}$-component equal to zero, the point $\boldsymbol{z}_{\boldsymbol{k}}^{\boldsymbol{j}-\boldsymbol{e}}$ lies on the boundary and the function $\psi_{\boldsymbol{k}}^{\boldsymbol{j}}$ is constant in one direction over the whole domain Ω, and it is of Haar-wavelet type for the non-zero indices (or index). In this situation the same estimate (23) holds with, e.g. if $j_1 = 0$,

$$|u| = \max \left| \frac{\partial^2 u(\boldsymbol{x})}{\partial x_2 \cdots \partial x_3} \right|.$$

For $\boldsymbol{j} = \mathbf{o}$ the relation (23) is trivially satisfied. Hence, the estimate (23) holds for $\boldsymbol{j} \ge \mathbf{o}$ if we use the seminorm (21), and we find

$$|a_{\boldsymbol{j},\boldsymbol{k}}| \le 2^{-\frac{3}{2}}\, 2^{-\frac{3}{2}|\boldsymbol{j}|}\, |u|.$$

$$\|u_{\boldsymbol{j}}\|^2 = \sum_{\boldsymbol{k}} |a_{\boldsymbol{j}\boldsymbol{k}}|^2 \le \sum_{\boldsymbol{k}} 2^{-3|\boldsymbol{j}|-3}\, |u|^2 = 2^{-2|\boldsymbol{j}|-3}\, |u|^2,$$

so that

$$\|u_{\boldsymbol{j}}\| \le 2^{|\boldsymbol{j}|-3/2}|u|,$$

which leads to (21), and

$$\begin{aligned}\|u - R_{\boldsymbol{n}} u\|^2 &= \sum_{\substack{j_1 > n_1 \\ \text{or } \cdots \text{ or} \\ j_3 > n_3}} \|u_{\boldsymbol{j}}\|^2 \le \sum_{\substack{j_1 > n_1 \\ j_2 \ge 0 \\ j_3 \ge 0}} + \cdots + \sum_{\substack{j_1 \ge 0 \\ j_2 \ge 0 \\ j_3 > n_3}} 2^{-2|\boldsymbol{j}|-3}|u|^2 \\ &\le 3^{-3}\, 2\, \left(2^{-2n_1} + 2^{-2n_2} + 2^{-2n_3}\right) |u|^2 .\end{aligned}$$

and it follows that

$$\|u - R_{\boldsymbol{n}} u\| \le \left(\frac{2}{3^3}\right)^{1/2} \left(2^{-n_1} + 2^{-n_2} + 2^{-n_3}\right) |u| = \frac{1}{3}\sqrt{\frac{2}{3}}\, (h_1 + h_2 + h_3)\, |u| .$$

□

If we have no further a-priori knowledge about u, the most efficient approximation will be one with $h_1 = h_2 = h_3$ because this equalises the three main terms in the error bound. We see that

$$R_{\boldsymbol{n}} = \sum_{\boldsymbol{j} \le \boldsymbol{n}} Q_{\boldsymbol{j}} ,$$

and the truncation error for $u - R_{\boldsymbol{n}} u$ is neither particularly promising nor surprising: the major part of the error is produced by the largest meshwidth: $(\max(h_1, h_2, h_3))^{3/2}$, whereas the total number of degrees of freedom for an element in $V_{\boldsymbol{n}}$ is $2^{|\boldsymbol{n}|}$.

Following the idea of sparse grids, as introduced for finite elements in [3, 9], a better accuracy per degree of freedom is obtained for the approximation operator

$$\hat{R}_m = \sum_{|\boldsymbol{j}| \le m} Q_{\boldsymbol{j}} \tag{24}$$

with $m \in \mathbb{Z}$.

Theorem 2.3 For the approximation operator (24) we have the truncation error estimate

$$\|u - \hat{R}_m u\| < M(\varepsilon) 2^{-(3-\varepsilon)m/2} |u| = M(\varepsilon)\, (h_1 h_2 h_3)^{(3-\varepsilon)/2}\, |u| . \tag{25}$$

for some arbitrary small constant ε and a constant $M(\varepsilon)$, depending on ε.

Proof: Following the same lines as in Theorem 2.2, and because $\|u_{\boldsymbol{j}}\|^2 \le 2^{-3|\boldsymbol{j}|}|u|$, we get

$$\begin{aligned}\|u - \hat{R}_m u\|^2 &= \textstyle\sum_{|\boldsymbol{j}|>m} \|u_{\boldsymbol{j}}\|^2 \\ &\le |u|^2 \textstyle\sum_{|\boldsymbol{j}|>m} 2^{-3|\boldsymbol{j}|} = |u|^2 \sum_{l>m} \sum_{|\boldsymbol{j}|=l} 2^{-3|\boldsymbol{j}|} \\ &= |u|^2 \textstyle\sum_{l>m} \frac{(l+1)(l+2)}{2} 2^{-\varepsilon l} 2^{-(3-\varepsilon)l} \\ &\le |u|^2 M(\varepsilon)^2 \textstyle\sum_{l>m} 2^{-(3-\varepsilon)l} \\ &= |u|^2 M(\varepsilon)^2 2^{-m(3-\varepsilon)}\end{aligned} \tag{26}$$

Hence

$$\|u - \hat{R}_m u\| \le M(\varepsilon) 2^{-m(3-\varepsilon)/2} |u| \tag{27}$$

where $2^{-m} = h_1 h_2 h_3$ is the volume of the smallest cells in the sparse grid used for the approximation of u. □

In (22) all h_j need to be small and in (25) only their product. This means that for convergence in (22) all meshsizes should tend to zero, whereas in (25) only the area should vanish. Further, the estimate (25) is of the same order of accuracy as (22), except for a logarithmic small factor. However, the number of degrees of freedom for the approximation (25) is significantly less. Namely, in the unit cube, for $R_{\boldsymbol{n}}u$ the number of degrees of freedom is $2^{|\boldsymbol{n}|}$, whereas for $\hat{R}_m u$ it is $(m^2+m+2)2^m-1$. Because significantly less degrees of freedom are involved in the approximation $\hat{R}_m u$ than in the approximation of $R_{(m,m,m)}u$, i.e. less coefficients $a_{\boldsymbol{j},\boldsymbol{k}}$ and less gridpoints $\boldsymbol{z}_{\boldsymbol{j},\boldsymbol{k}}$, following [3], we call the approximation $\hat{R}_m u$ the *sparse grid approximation* and

$$\Omega_m^* = \left\{ \boldsymbol{z}_{\boldsymbol{j},\boldsymbol{k}} \mid \boldsymbol{z}_{\boldsymbol{j},\boldsymbol{k}} \in \Omega_{\boldsymbol{j}}^*, |j| \leq m \right\}$$

is the *sparse grid* or *sparse box grid* for this approximation on level m.

In this paper we are interested in the approximate solution of PDEs discretised on a sparse grid, i.e. we are looking for an approximation of the solution of these equations in the space

$$S_m(\mathbb{R}^3) = \bigoplus_{|\boldsymbol{n}|\leq m} V_{\boldsymbol{n}} = \bigoplus_{|\boldsymbol{n}|\leq m} W_{\boldsymbol{n}},$$

or, for $\Omega = (0,1)^3$, in the space

$$S_m(\Omega) = \bigoplus_{0\leq|\boldsymbol{n}|\leq m} V_{\boldsymbol{n}} = V_{\boldsymbol{0}} \oplus \bigoplus_{\boldsymbol{0}\leq|\boldsymbol{n}|\leq m} W_{\boldsymbol{n}}.$$

We call $S_m(\Omega)$ the *m-th level sparse-grid space.*

3 A multigrid algorithm in three dimensions

The principle of multigrid for the solution of the discrete equation

$$L_h\, u_h = f_h$$

is that the high frequencies in the error are reduced by relaxation on a fine grid, whereas the low frequencies are taken care of by coarse-grid discrete equations. The classical coarse grid correction (CGC) step is described by

$$u^{(\text{new})} = u^{(\text{old})} + P_{hH} L_H^{-1} R_{Hh} \left(f_h - L_h u^{(\text{old})} \right),$$

where L_H is the coarse-grid discrete operator and P_{hH} and R_{Hh} are the grid-transfer operators from the coarse-to-the-fine and fine-to-the-coarse grid respectively. Usually the coarse-grid mesh size is twice the mesh size on the next finer grid. The coarse grid problem is approximately solved by means of the recursive application of the same algorithm on the coarser level. In this classical procedure a linearly ordered sequence of fine and coarse discretisations is required.

In the case of our sparse-grid finite-volume approximation, a discretisation should exist for all grids $\Omega_{\boldsymbol{n}}$, $|\boldsymbol{n}| \leq m$, fine and coarse. On each of these grids we can obtain approximations to $u_{\boldsymbol{n}} \in V_{\boldsymbol{n}}$, the solution of the discrete problem

$$L_{\boldsymbol{n}}\, u_{\boldsymbol{n}} = f_{\boldsymbol{n}} \quad \text{on} \quad \Omega_{\boldsymbol{n}}. \tag{28}$$

These discretisations, however, don't offer an ordered sequence. Nevertheless, the multidimensional wavelet decomposition of $u_{\boldsymbol{n}} \in V_{\boldsymbol{n}}$,

$$u_{\boldsymbol{n}} = v_{\mathbf{0}} + \sum_{\boldsymbol{j} \leq \boldsymbol{n}} w_{\boldsymbol{j}}, \quad \text{with } w_{\boldsymbol{j}} \in W_{\boldsymbol{j}},$$

allows us to distinguish a high-frequency component, $w_{\boldsymbol{n}}$, that cannot be represented on coarser grids, and all other components, $v_{\mathbf{0}}$ and $w_{\boldsymbol{j}}$, $\boldsymbol{j} \leq \boldsymbol{n}$, $\boldsymbol{j} \neq \boldsymbol{n}$, which can be present in coarser grid representations. Therefore we may consider the grid $\Omega_{\boldsymbol{n}}$ to be solely responsible for the accurate (and efficient) representation of $w_{\boldsymbol{n}}$. This component is clearly a high-frequency function (in fact a checkerboard-type function), of which an error can be efficiently reduced by a simple relaxation procedure as e.g. damped Jacobi.

The decomposition (12) in Theorem 2.1 shows us how a CGC can be obtained from these coarser grids in $\Omega_{\boldsymbol{n}-\boldsymbol{e}_j}$, $j = 1, 2, 3$,

$$\begin{aligned} u_{\boldsymbol{n}}^{(\text{new})} = u_{\boldsymbol{n}}^{(\text{old})} \quad &+ \sum_{j=1,2,3} P_{\boldsymbol{n},\boldsymbol{n}-\boldsymbol{e}_j} L_{\boldsymbol{n}-\boldsymbol{e}_j}^{-1} R_{\boldsymbol{n}-\boldsymbol{e}_j,\boldsymbol{n}}\, r_{\boldsymbol{n}} \\ &- \sum_{j=1,2,3} P_{\boldsymbol{n},\boldsymbol{n}-\boldsymbol{e}+\boldsymbol{e}_j} L_{\boldsymbol{n}-\boldsymbol{e}+\boldsymbol{e}_j}^{-1} R_{\boldsymbol{n}-\boldsymbol{e}+\boldsymbol{e}_j,\boldsymbol{n}}\, r_{\boldsymbol{n}} \\ &+ P_{\boldsymbol{n},\boldsymbol{n}-\boldsymbol{e}} L_{\boldsymbol{n}-\boldsymbol{e}}^{-1} R_{\boldsymbol{n}-\boldsymbol{e},\boldsymbol{n}}\, r_{\boldsymbol{n}}, \end{aligned} \tag{29}$$

with

$$r_{\boldsymbol{n}} = f_{\boldsymbol{n}} - L_{\boldsymbol{n}} u_{\boldsymbol{n}}^{(\text{old})}. \tag{30}$$

Here we denote by $R_{\boldsymbol{m},\boldsymbol{n}} : V_{\boldsymbol{n}} \to V_{\boldsymbol{m}}$, $\boldsymbol{m} \leq \boldsymbol{n}$, the restriction operator defined by $R_{\boldsymbol{m},\boldsymbol{n}} u_{\boldsymbol{n}} = R_{\boldsymbol{m}} u_{\boldsymbol{n}}$ for all $u_{\boldsymbol{n}} \in V_{\boldsymbol{n}} \subset L^2(\Omega)$. The prolongation operator $P_{\boldsymbol{n},\boldsymbol{m}} : V_{\boldsymbol{m}} \to V_{\boldsymbol{n}}$ can be defined e.g. as the adjoint of $R_{\boldsymbol{m},\boldsymbol{n}}$.

The third remark following Theorem 2.1 shows how the two- or one-dimensional case can be treated similarly and we see that -for the one-dimensional case- our approach reduces to the classical scheme.

The approach (29) would imply three coarser levels to be active for a CGC, and -as was shown in the remark after Theorem 2.1- we can do with only one coarser level by deriving the information on the levels $|\boldsymbol{n}| - 3$ and $|\boldsymbol{n}| - 2$ from the information on level $|\boldsymbol{n}| - 1$. If we consider the corrections from level $|\boldsymbol{n}| - 1$,

$$c_{\boldsymbol{n}-\boldsymbol{e}_j} = L_{\boldsymbol{n}-\boldsymbol{e}_j}^{-1} R_{\boldsymbol{n}-\boldsymbol{e}_j,\boldsymbol{n}}\, r_{\boldsymbol{n}}, \quad j = 1, 2, 3, \tag{31}$$

as approximating a single (but unknown) correction function $c_{\boldsymbol{n}} \in V_{\boldsymbol{n}}$, the corrections from the levels $|\boldsymbol{n}| - 2$ and $|\boldsymbol{n}| - 3$ can be computed as the mean values

$$c_{\boldsymbol{n}-\boldsymbol{e}+\boldsymbol{e}_j} = \frac{1}{2}\left(R_{\boldsymbol{n}-\boldsymbol{e}+\boldsymbol{e}_j,\boldsymbol{n}-\boldsymbol{e}_{j+1}} c_{\boldsymbol{n}-\boldsymbol{e}_{j+1}} + R_{\boldsymbol{n}-\boldsymbol{e}+\boldsymbol{e}_j,\boldsymbol{n}-\boldsymbol{e}_{j-1}} c_{\boldsymbol{n}-\boldsymbol{e}_{j-1}} \right), \tag{32}$$

$j = 1, 2, 3$, and

$$c_{\boldsymbol{n}-\boldsymbol{e}} = \frac{1}{3} \sum_{j=1,2,3} R_{\boldsymbol{n}-\boldsymbol{e},\boldsymbol{n}-\boldsymbol{e}+\boldsymbol{e}_j} c_{\boldsymbol{n}-\boldsymbol{e}+\boldsymbol{e}_j}. \tag{33}$$

This is justified by the fact that the restrictions are commutative, i.e.

$$\boldsymbol{m} \leq \boldsymbol{n} \leq \boldsymbol{l} \quad \Rightarrow \quad R_{\boldsymbol{m},\boldsymbol{n}} R_{\boldsymbol{n},\boldsymbol{l}} = R_{\boldsymbol{m},\boldsymbol{l}}$$

and the following (trivial) lemma.

Lemma 3.1 If all discrete operators $L_{\boldsymbol{n}}$ are stable and relatively consistent, i.e.

$$\|R_{\boldsymbol{n},\boldsymbol{n}+\boldsymbol{e}_j} L_{\boldsymbol{n}+\boldsymbol{e}_j} - L_{\boldsymbol{n}} R_{\boldsymbol{n},\boldsymbol{n}+\boldsymbol{e}_j}\| \leq \mathcal{O}(2^{-|\boldsymbol{n}|_p})$$

then

$$\|c_{\boldsymbol{n}-\boldsymbol{e}_j} - R_{\boldsymbol{n}-\boldsymbol{e}_j,\boldsymbol{n}} c_{\boldsymbol{n}}\| \leq \mathcal{O}(2^{-|\boldsymbol{n}|_p}) \ .$$

The consistent discretisations can be derived e.g. from the fine grid discretisation $L_{\boldsymbol{n}}$ by taking the Galerkin approximation

$$L_{\boldsymbol{n}-\boldsymbol{e}_j} = R_{\boldsymbol{n}-\boldsymbol{e}_j,\boldsymbol{n}} L_{\boldsymbol{n}} P_{\boldsymbol{n},\boldsymbol{n}-\boldsymbol{e}_j} \ .$$

If the three corrections $c_{\boldsymbol{n}-\boldsymbol{e}_j}$ were all restrictions of the (unknown) correction $c_{\boldsymbol{n}} \in V_{\boldsymbol{n}}$ indeed, then $R_{\boldsymbol{n}-\boldsymbol{e}+\boldsymbol{e}_j,\boldsymbol{n}-\boldsymbol{e}_{j+1}} c_{\boldsymbol{n}-\boldsymbol{e}_{j+1}}$ and $R_{\boldsymbol{n}-\boldsymbol{e}+\boldsymbol{e}_j,\boldsymbol{n}-\boldsymbol{e}_{j-1}} c_{\boldsymbol{n}-\boldsymbol{e}_{j-1}}$ would both have delivered the same result, viz., $R_{\boldsymbol{n}-\boldsymbol{e}+\boldsymbol{e}_j,\boldsymbol{n}}\, c_{\boldsymbol{n}}$. This gives us the possibility to check how well such a function $c_{\boldsymbol{n}}$ can be determined, by monitoring the quantities, $j = 1, 2, 3$,

$$d_{\boldsymbol{n}-\boldsymbol{e}+\boldsymbol{e}_j} = \frac{1}{2}\left(R_{\boldsymbol{n}-\boldsymbol{e}+\boldsymbol{e}_j,\boldsymbol{n}-\boldsymbol{e}_{j+1}} c_{\boldsymbol{n}-\boldsymbol{e}_{j+1}} - R_{\boldsymbol{n}-\boldsymbol{e}+\boldsymbol{e}_j,\boldsymbol{n}-\boldsymbol{e}_{j-1}} c_{\boldsymbol{n}-\boldsymbol{e}_{j-1}}\right) . \tag{34}$$

Summarising, our multigrid algorithm now reads:

$$\begin{aligned} u_{\boldsymbol{n}}^{(i+1)} = u_{\boldsymbol{n}}^{(i)} \ &+ \ \textstyle\sum_{j=1,2,3} P_{\boldsymbol{n},\boldsymbol{n}-\boldsymbol{e}_j}\, c_{\boldsymbol{n}-\boldsymbol{e}_j} \\ &- \ \textstyle\sum_{j=1,2,3} P_{\boldsymbol{n},\boldsymbol{n}-\boldsymbol{e}+\boldsymbol{e}_j}\, c_{\boldsymbol{n}-\boldsymbol{e}+\boldsymbol{e}_j} \\ &+ \ P_{\boldsymbol{n},\boldsymbol{n}-\boldsymbol{e}}\, c_{\boldsymbol{n},\boldsymbol{n}-\boldsymbol{e}} \ , \end{aligned} \tag{35}$$

where the corrections are given by (31), (32) and (33). This appears to be much similar to an multigrid algorithm for semi-coarsening, proposed by Mulder in [7]. The main difference being that Mulder computes an approximation on the full grid $R_{\boldsymbol{n}}$, whereas we compute the sparse grid approximation $\hat{R}_m$.

The result of our algorithm is a solution on a sparse grid, i.e. a set of approximate solutions, viz. $\{u_{\boldsymbol{n}} \mid |\boldsymbol{n}| = m\}$, that are the solutions of the discrete equations $L_{\boldsymbol{n}} u_{\boldsymbol{n}} = f_{\boldsymbol{n}}$. All approximations $u_{\boldsymbol{n}}$ representing the same solution u of the continuous problem, we assume that they approximate the $L^2(\Omega)$-projection of u in $V_{\boldsymbol{m}} = V_{(m,m,m)}$. To approximate this $R_{\boldsymbol{m}} u \in V_{\boldsymbol{m}}$, we can construct a unique function $u_{\boldsymbol{m}} \in V_{\boldsymbol{m}}$ by means of the recursive interpolation formula that immediately follows from Theorem 2.1:

$$u_{\boldsymbol{k}} = \sum_{j=1,2,3} \left(u_{\boldsymbol{k}-\boldsymbol{e}_j} - u_{\boldsymbol{k}-\boldsymbol{e}+\boldsymbol{e}_j}\right) + u_{\boldsymbol{k}-\boldsymbol{e}} \ , \tag{36}$$

where $\mathbf{o} \leq \boldsymbol{k} \leq \boldsymbol{m}$, $|\boldsymbol{k}| = m+1, \ldots, 3m$; $u_{\boldsymbol{k}-\boldsymbol{e}_j}$ are the functions computed in the previous recursion cycle and $u_{\boldsymbol{k}-\boldsymbol{e}+\boldsymbol{e}_j}$ and $u_{\boldsymbol{k}-\boldsymbol{e}}$ are approximations (possibly) derived as (32) and (33). In this way we finally obtain the unique representation

$$u_{\boldsymbol{m}} = v_{\mathbf{o}} + \sum_{0 \leq |\boldsymbol{k}| \leq m} w_{\boldsymbol{k}} \tag{37}$$

of $u_{\boldsymbol{m}} \in S_m(\Omega) \subset V_{(m,m,m)}(\Omega)$. This representation can be considered as the computed solution.

The same construction can be realised by a 'decomposition and reconstruction' algorithm as used in wavelet theory [2]. Then the available approximate solutions $\{u_{\boldsymbol{n}}\}$ are decomposed into their components $v_{\mathbf{o}}$ and $\{w_{\boldsymbol{k}}\}$ by

$$v_{\mathbf{o}} = \frac{\sum_{|\boldsymbol{n}|=m} R_{\mathbf{o}} u_{\boldsymbol{n}}}{\sum_{|\boldsymbol{n}|=m} 1} \qquad \text{and} \qquad w_{\boldsymbol{k}} = \frac{\sum_{|\boldsymbol{n}|=m} Q_{\boldsymbol{k}} u_{\boldsymbol{n}}}{\sum_{|\boldsymbol{n}|=m} 1}$$

and the reconstruction is performed by (37). This can conveniently be performed by a kind of a 'pyramid algorithm'. This will be reported in a later paper.

In practice, by the choice of the discrete operator our assumption that the $L^2(\Omega)$-projection of u was indeed consistently approximated on $V_{\boldsymbol{n}}$, may not necessarily hold, and it can be checked by a monitor as (34). Now, e.g., the corresponding erroneous components might be removed from the sum (37).

In the light of the treatment in Section 2 it is clear what restrictions and prolongations can be used between the different grids in the multigrid process. Because $V_{\boldsymbol{n}} \subset L^2(\Omega)$, the obvious restriction $R_{\boldsymbol{n}-\boldsymbol{e}_j,\boldsymbol{n}}$ is the $L^2(\Omega)$-projection onto $V_{\boldsymbol{n}-\boldsymbol{e}_j}$:

$$R_{\boldsymbol{n}-\boldsymbol{e}_j,\boldsymbol{n}} = R_{\boldsymbol{n}-\boldsymbol{e}_j}\,.$$

This makes the diagram for the restrictions commutative: for any $\boldsymbol{l} \leq \boldsymbol{m} \leq \boldsymbol{n}$ we have $R_{\boldsymbol{l},\boldsymbol{m}} R_{\boldsymbol{m},\boldsymbol{n}} = R_{\boldsymbol{l},\boldsymbol{n}}$.

An obvious prolongation can be the transposed restriction

$$P_{\boldsymbol{n},\boldsymbol{n}-\boldsymbol{e}_j} = R^T_{\boldsymbol{n}-\boldsymbol{e}_j,\boldsymbol{n}}\,.$$

However, this prolongation being of low order, it may be more appropriate to consider higher order prolongations. Such prolongations can always be represented by an additional operator $B_{\boldsymbol{n}} : V_{\boldsymbol{n}} \to V_{\boldsymbol{n}}$ so that we have

$$P_{\boldsymbol{n},\boldsymbol{n}-\boldsymbol{e}_j} = B_{\boldsymbol{n}} R^T_{\boldsymbol{n}-\boldsymbol{e}_j}\,.$$

Here we will not elaborate on the different possibilities for $B_{\boldsymbol{n}}$.

The algorithm (35) shows that all relaxation processes for $u_{\boldsymbol{n}}$ on one and the same level $m = |\boldsymbol{n}|$ can be made in parallel. The cycling between the different (scalar) levels can be made as for the classical multigrid method: we can distinguish between V-, W- or F-cycles. However, in order to prove that the convergence of our multigrid-method is independent of the meshwidth, we now have to take into account that all aspect ratios will appear in the discretisations used.

4 Convergence analysis

Here we first summarise some results of Fourier analysis for more-dimensional discrete approximations and then we apply this to compute the convergence rate of our sparse-grid multiple-grid methods for the solution of the anisotropic Poisson equation. The approach is different from the usual treatment of Fourier analysis for multigrid for finite difference methods for the following reasons. First, in view of the discretisation of conservation laws and divergence problems, we study nested box grids. This implies that mesh points in the coarse grids do not appear in the fine grids as well. The nesting of the (box) grids is different from the usual nesting of the (finite difference or finite element) grids. Second, we do not consider the usual sequences of fine and coarser meshes for multigrid methods, but we allow d-dimensional ($d = 2, 3$) sparse grids.

Fourier analysis is one of the common tools to analyse linear constant coefficient problems on regular grids, and it is particularly useful if the treatment of boundary conditions can be neglected.

In Section 4.1 we describe general tools that can be used for the Fourier analysis of functions defined on more-dimensional box grids. The definitions and theorems provide

a useful machinery for the application of local mode analysis for the multigrid box-methods.

In Section 4.2 we apply tools to analyse the multigrid algorithm introduced in section 3. The technical preparations in 4.1 allow us to be brief and clear in this treatment.

4.1 Fourier analysis for box grids

For $u \in L^2(\mathbb{R}^3)$ we introduce its Fourier Transform (FT) $\hat{u}$, scaled as

$$\hat{u}(\boldsymbol{\omega}) = (2\pi)^{-3/2} \int_{\mathbb{R}^3} e^{-i\boldsymbol{x}\boldsymbol{\omega}}\, u(\boldsymbol{x})\, d\boldsymbol{x}\,. \tag{38}$$

Then we know that $\hat{u} \in L^2(\mathbb{R}^3)$, and a back-transformation formula is available,

$$\check{u}(\boldsymbol{x}) = (2\pi)^{-3/2} \int_{\mathbb{R}^3} e^{+i\boldsymbol{x}\boldsymbol{\omega}}\, \hat{u}(\boldsymbol{\omega})\, d\boldsymbol{\omega}\,, \tag{39}$$

such that $\check{u}(\boldsymbol{x}) = u(\boldsymbol{x})$ almost everywhere on $\mathbb{R}^3$. Moreover, $\hat{u} \in L^2(\mathbb{R}^3)$ and Parseval's equality holds: $\|u\|_{L^2(\mathbb{R}^3)} = \|\hat{u}\|_{L^2(\mathbb{R}^3)}$.

We are interested in the Fourier transformation for an infinite set of equally spaced data. In this case the FT of such a "grid function" is a periodic function (a function defined on a torus). Therefore we introduce a few definitions.

Let $\boldsymbol{h} \in \mathbb{R}^3$, $\boldsymbol{h} > \mathbf{o}$, be given, then the *$\boldsymbol{h}$-periodisation* of a function $u : \mathbb{R}^3 \to \mathbb{C}$ is defined by

$$\tilde{u}(\boldsymbol{x}) = \sum_{\boldsymbol{k} \in \mathbb{Z}^3} u(\boldsymbol{x} - \boldsymbol{k}\boldsymbol{h}), \tag{40}$$

where $\boldsymbol{k}\boldsymbol{h} = (k_1 h_1, k_2 h_2, k_3 h_3)$. We also introduce a notation for the *three-dimensional torus*

$$T_{\boldsymbol{h}} = (-\pi/\boldsymbol{h}, \pi/\boldsymbol{h}] = (-\pi/h_1, \pi/h_1] \times \ldots \times (-\pi/h_3, \pi/h_3]. \tag{41}$$

Further we need the functions Π and Sinc, [1, pp.62,67] on $\mathbb{R}^3$,

$$\Pi(\boldsymbol{x}) = \begin{cases} 1 & \text{for } |x_i| < 1/2\,, \quad 1 \le i \le 3, \\ 0 & \text{otherwise}\,, \end{cases} \tag{42}$$

and

$$\text{Sinc } x = \prod_{i=1}^{i=3} \frac{\sin \pi x_i}{\pi x_i}\,.$$

Using the relations mentioned in [1, p.98] we find

$$\hat{\Pi}(\boldsymbol{\omega}) = (2\pi)^{-3/2} \prod_{i=1,2,3} \text{sinc}\,(\frac{\omega_i}{2\pi}) = (2\pi)^{-3/2}\, \text{Sinc}\,(\frac{\boldsymbol{\omega}}{2\pi})\,. \tag{43}$$

For an $\boldsymbol{h} \in \mathbb{R}^3$, $\boldsymbol{h} > \mathbf{o}$, we define the *dilation operator* $D_{\boldsymbol{h}} : L^2(\mathbb{R}^3) \to L^2(\mathbb{R}^3)$ by

$$D_{\boldsymbol{h}} f(\boldsymbol{x}) = h^{-3/2} f(\boldsymbol{x}\boldsymbol{h})\,, \tag{44}$$

where $h = (h_1 h_2 h_3)^{1/3}$, and the *convolution operator*, $\star$, by

$$(f \star g)(\boldsymbol{x}) = (2\pi)^{-3/2} \int_{\mathbb{R}^3} f(\boldsymbol{y})\, g(\boldsymbol{x} - \boldsymbol{y})\, d\boldsymbol{y}\,. \tag{45}$$

We now know that

$$\widehat{D_{\boldsymbol{h}}} = D_{1/\boldsymbol{h}}\, \hat{f} \quad \text{and} \quad \widehat{f \star g}\,(\boldsymbol{\omega}) = \hat{f}(\boldsymbol{\omega}) \cdot \hat{g}(\boldsymbol{\omega})\,. \tag{46}$$

GRID FUNCTIONS.

Here we introduce notations for the different types of grids and gridfunctions.

Definition 4.1 For a fixed *mesh parameter* $\boldsymbol{h}\in\mathbb{R}^3$, $\boldsymbol{h} > \mathbf{o}$, and for $\boldsymbol{j}\in\mathbb{Z}^3$, we define an *elementary cell* by $\Omega_{\boldsymbol{h},\boldsymbol{j}} = \{\boldsymbol{x} \mid \boldsymbol{j}\boldsymbol{h} < \boldsymbol{x} < (\boldsymbol{j}+\boldsymbol{e})\boldsymbol{h}\}$, the volume of the cell is denoted by $h^3 = h_1 \cdot h_2 \cdot h_3$, and the *box-grid* is defined by $\Omega_{\boldsymbol{h}} = \{\Omega_{\boldsymbol{h},\boldsymbol{j}} \mid \boldsymbol{j}\in\mathbb{Z}^3\}$. The regular infinite three-dimensional *grid* of vertices $\mathbb{Z}_{\boldsymbol{h}}$ is defined by $\mathbb{Z}_{\boldsymbol{h}} = \{\boldsymbol{j}\boldsymbol{h} \mid \boldsymbol{j}\in\mathbb{Z}^3\}$, which should be well distinguished from the *shifted grid* which is defined by $\mathbb{Z}^\star_{\boldsymbol{h}} = \{(\boldsymbol{j}+\boldsymbol{e}/2)\boldsymbol{h} \mid \boldsymbol{j}\in\mathbb{Z}^3\}$.

Notice the relation with the grids as defined in Section 2.2: $\Omega_{\boldsymbol{n}}$ can be considered as a special case of $\Omega_{\boldsymbol{h}}$, and $\Omega^\star_{\boldsymbol{n}}$ as a special case of $\mathbb{Z}^\star_{\boldsymbol{h}}$.

Definition 4.2 A complex or a real *grid function* $u^\bullet_{\boldsymbol{h}}$ is a mapping $\mathbb{Z}_{\boldsymbol{h}} \to \mathbb{C}$, or $\mathbb{Z}_{\boldsymbol{h}} \to \mathbb{R}$, and a *shifted* or *box-grid function* $u^\star_{\boldsymbol{h}}$ is a mapping $\mathbb{Z}^\star_{\boldsymbol{h}} \to \mathbb{C}$ or $\mathbb{Z}^\star_{\boldsymbol{h}} \to \mathbb{R}$.

The vector space of such gridfunctions we denote by $l(\mathbb{Z}_{\boldsymbol{h}})$ or $l(\mathbb{Z}^\star_{\boldsymbol{h}})$, or briefly, by l. For any $p \geq 1$ the space $l(\mathbb{Z}_{\boldsymbol{h}})$ can be provided with a norm $\|\cdot\|_p$

$$\|u^\bullet_{\boldsymbol{h}}\|_p = (h^3 \sum_{\boldsymbol{j}\in\mathbb{Z}^3} |u^\bullet_{\boldsymbol{h}}(\boldsymbol{j}\boldsymbol{h})|^p)^{1/p}. \tag{47}$$

For a fixed p, all grid functions with a finite norm $\|\cdot\|_p$ form a Banach space denoted by $l^p(\mathbb{Z}_{\boldsymbol{h}})$. For $p = 2$ we know that $l^2(\mathbb{Z}_{\boldsymbol{h}})$ is a Hilbert space with the inner product,

$$< u^\bullet_{\boldsymbol{h}}, v^\bullet_{\boldsymbol{h}} >_{l^2(\mathbb{Z}_{\boldsymbol{h}})} = h^3 \sum_{\boldsymbol{j}\in\mathbb{Z}^3} u^\bullet_{\boldsymbol{h}}(\boldsymbol{j}\boldsymbol{h})\overline{v^\bullet_{\boldsymbol{h}}}(\boldsymbol{j}\boldsymbol{h}) \quad \text{with} \quad u^\bullet_{\boldsymbol{h}}, v^\bullet_{\boldsymbol{h}}\in\mathbb{Z}_{\boldsymbol{h}}. \tag{48}$$

Similar definitions are given for $l(\mathbb{Z}^\star_{\boldsymbol{h}})$:

$$< u^\star_{\boldsymbol{h}}, v^\star_{\boldsymbol{h}} >_{l^2(\mathbb{Z}^\star_{\boldsymbol{h}})} = h^3 \sum_{\boldsymbol{z}\in\mathbb{Z}^\star_{\boldsymbol{h}}} u^\star_{\boldsymbol{h}}(\boldsymbol{z})\overline{v^\star_{\boldsymbol{h}}}(\boldsymbol{z}) \quad \text{with} \quad u^\star_{\boldsymbol{h}}, v^\star_{\boldsymbol{h}}\in\mathbb{Z}^\star_{\boldsymbol{h}}. \tag{49}$$

Definition 4.3 The *direct restriction* $R^\bullet_{\boldsymbol{h}} : L^2(\mathbb{R}^3) \to l(\mathbb{Z}_{\boldsymbol{h}})$ is the operator that associates with a continuous $u\in L^2(\mathbb{R}^3)$ the corresponding grid function on the grid $\mathbb{Z}_{\boldsymbol{h}}$, defined by

$$(R^\bullet_{\boldsymbol{h}}u)(\boldsymbol{j}\boldsymbol{h}) = u(\boldsymbol{j}\boldsymbol{h}), \quad \forall \boldsymbol{j}\in\mathbb{Z}^3, \tag{50}$$

and the *direct restriction* $R^\star_{\boldsymbol{h}} : L^2(\mathbb{R}^3) \to l(\mathbb{Z}^\star_{\boldsymbol{h}})$ on the shifted grid $\mathbb{Z}^\star_{\boldsymbol{h}}$ is defined by

$$(R^\star_{\boldsymbol{h}}u)((\boldsymbol{j}+\boldsymbol{e}/2)\boldsymbol{h}) = u((\boldsymbol{j}+\boldsymbol{e}/2)\boldsymbol{h}), \quad \forall \boldsymbol{j}\in\mathbb{Z}^3. \tag{51}$$

In case of a discontinuous function we can replace u by $\breve{u}$ as defined in (39).

Definition 4.4 The *box-restriction* $R_{\boldsymbol{h}} : L^2(\mathbb{R}^3) \to L^2(\mathbb{R}^3)$ is the L^2-projection on the piecewise constant functions on $\Omega_{\boldsymbol{h}}$, defined by (cf. equation (6))

$$(R_{\boldsymbol{h}}u)(\boldsymbol{x}) = h^{-3} \int_{\Omega_{\boldsymbol{h},\boldsymbol{j}}} u(\boldsymbol{z})\, d\boldsymbol{z} \quad \forall \boldsymbol{x}\in\Omega_{\boldsymbol{h},\boldsymbol{j}}. \tag{52}$$

The *box-restriction* $R^B_{\boldsymbol{h}} : L^2(\mathbb{R}^3) \to l(\mathbb{Z}^\star_{\boldsymbol{h}})$ is defined by $R^B_{\boldsymbol{h}} = R^\star_{\boldsymbol{h}}R_{\boldsymbol{h}}$; it associates the mean value of u on a cell $\Omega_{\boldsymbol{h},\boldsymbol{j}}$ with the nodal value at the centre of $\Omega_{\boldsymbol{h},\boldsymbol{j}}$.

The box-restriction $R_h^B u$ should be well distinguished from $R_h^\star u$. However, the $L^2(\Omega)$-projection $R_h u$ in (52) and the restriction $R_h^B u$ in (51) are conveniently related to each other by

$$R_h u = \left(\frac{2\pi}{h}\right)^{3/2} R_h^\star \left((D_h \Pi) \star u\right). \tag{53}$$

THE FOURIER TRANSFORM OF A GRID FUNCTION.
Let $u_h^\bullet : \mathbb{Z}_h \to \mathbb{C}$ be a grid function. We give the following

Definition 4.5 The Fourier transform $\widehat{u_h^\bullet} \in L^2(T_h)$ of a grid function $u_h^\bullet \in l^2(\mathbb{Z}_h)$ is a function $T_h \to \mathbb{C}$, defined by

$$\widehat{u_h^\bullet}(\omega) = \left(\frac{h}{\sqrt{2\pi}}\right)^3 \sum_{j \in \mathbb{Z}^3} e^{-ijh\omega}\, u_h^\bullet(jh). \tag{54}$$

The inverse transformation is given by

$$u_h^\bullet(jh) = \left(\frac{1}{\sqrt{2\pi}}\right)^3 \int_{\omega \in T_h} e^{+ijh\omega}\, \widehat{u_h^\bullet}(\omega)\, d\omega. \tag{55}$$

Let $u_h^\star : \mathbb{Z}_h^\star \to \mathbb{C}$ be a shifted grid function, then we have

Definition 4.6 The Fourier transform $\widehat{u_h^\star} \in L^2(T_h)$ of a shifted grid function $u_h^\star \in l^2(\mathbb{Z}_h^\star)$ is a function $T_h \to \mathbb{C}$, defined by

$$\widehat{u_h^\star}(\omega) = \left(\frac{h}{\sqrt{2\pi}}\right)^3 \sum_{j \in \mathbb{Z}^3} e^{-i(j+e/2)h\omega}\, u_h^\star((j+e/2)h). \tag{56}$$

Its inverse transformation is given by

$$u_h^\star((j+e/2)h) = \left(\frac{1}{\sqrt{2\pi}}\right)^3 \int_{\omega \in T_h} e^{+i(j+e/2)h\omega}\, \widehat{u_h^\star}(\omega)\, d\omega. \tag{57}$$

Remarks:

- We immediately see that $\widehat{u_h^\bullet}(\omega)$ is $[2\pi/h]$-*periodic*, whereas $\widehat{u_h^\star}(\omega)$ is $[2\pi/h]$-*antiperiodic*, i.e. $\widehat{u_h^\star}(\omega + 2\pi/h) = (-)^{|e|}\widehat{u_h^\star}(\omega)$.

- We denote the Fourier transforms also by

$$\widehat{u_h^\bullet} = \mathcal{F}(u_h^\bullet) \quad \text{or} \quad \widehat{u_h^\star} = \mathcal{F}(u_h^\star), \tag{58}$$

  i.e. we introduce the mapping $\mathcal{F} : l^2(\mathbb{Z}_h) \to L^2(T_h)$ or $\mathcal{F} : l^2(\mathbb{Z}_h^\star) \to L^2(T_h)$. At the end of this section we shall generalise this meaning of $\mathcal{F}$.

- By the Parseval equality we have

$$\|u_h^\bullet\|_2 = \|\widehat{u_h^\bullet}\|_{L^2(T_h)} \quad \text{and} \quad \|u_h^\star\|_2 = \|\widehat{u_h^\star}\|_{L^2(T_h)}. \tag{59}$$

  Hence the Fourier transformation operators $\mathcal{F}$: $l^2(\mathbb{Z}_h) \to L^2(T_h)$ and $\mathcal{F}$: $l^2(\mathbb{Z}_h^\star) \to L^2(T_h)$ are unitary operators.

- Because $e^{\bullet}_{\boldsymbol{h},\boldsymbol{\omega}} \equiv e^{\bullet}_{\boldsymbol{h},\boldsymbol{\omega}+2\pi\boldsymbol{k}/\boldsymbol{h}}$ or $e^{*}_{\boldsymbol{h},\boldsymbol{\omega}} \equiv (-)^{|\boldsymbol{ek}|} e^{*}_{\boldsymbol{h},\boldsymbol{\omega}+2\pi\boldsymbol{k}/\boldsymbol{h}}$, for all $\boldsymbol{k}\in\mathbb{Z}^3$, on a mesh of size $\boldsymbol{h}$ a frequency $\boldsymbol{\omega}$ cannot be distinguished from a frequency $\boldsymbol{\omega} + 2\pi\boldsymbol{k}/\boldsymbol{h}$. This phenomenon is called *aliasing* .

THE RELATION BETWEEN FTS OF A FUNCTION RESTRICTED TO DIFFERENT GRIDS. In this section we first present a few theorems associated with the different restrictions between two grids. We describe the relation between the FT of a continuous function defined on $\mathbb{R}^3$ and the FT of its restriction to the grid and then we show the relation between the FT of a fine grid function and the FT of its representation on a coarser grid. Next, we give the corresponding theorems for the prolongations.

Lemma 4.7 Let $u\in L^2(\mathbb{R}^3)$ be a continuous function with FT $\hat{u}$. Its restriction $u^{\bullet}_{\boldsymbol{h}}$ to the grid $\mathbb{Z}_{\boldsymbol{h}}$ is defined by (50). We have the following relation between $\hat{u}$ and $\widehat{u^{\bullet}_{\boldsymbol{h}}}$:

$$\widehat{u^{\bullet}_{\boldsymbol{h}}}(\boldsymbol{\omega}) = \sum_{\boldsymbol{k}\in\mathbb{Z}^3} \hat{u}(\boldsymbol{\omega} + 2\pi\boldsymbol{k}/\boldsymbol{h}), \tag{60}$$

i.e. $\widehat{u^{\bullet}_{\boldsymbol{h}}}$ is the $[2\pi/\boldsymbol{h}]$-periodisation of $\hat{u}$.
Proof:

$$\begin{aligned}\widehat{u^{\bullet}_{\boldsymbol{h}}}(\boldsymbol{\omega}) &= (\tfrac{\boldsymbol{h}}{2\pi})^d \textstyle\sum_j e^{-i\boldsymbol{jh\omega}} \sum_{\boldsymbol{k}} \int_{-\pi/\boldsymbol{h}}^{\pi/\boldsymbol{h}} e^{i\boldsymbol{jh}(\boldsymbol{y}+2\pi\boldsymbol{k}/\boldsymbol{h})}\hat{u}(\boldsymbol{y}+2\pi\boldsymbol{k}/\boldsymbol{h})d\boldsymbol{y} \\ &= (\tfrac{\boldsymbol{h}}{2\pi})^d \textstyle\sum_j e^{-i\boldsymbol{jh\omega}} \sum_{\boldsymbol{k}} \hat{u}(\boldsymbol{y}+2\pi\boldsymbol{k}/\boldsymbol{h})d\boldsymbol{y}\,.\end{aligned}$$

Using (54) and (55) we see that this equals $\sum_{\boldsymbol{k}\in\mathbb{Z}^d} \hat{u}(\boldsymbol{\omega} + 2\pi\boldsymbol{k}/\boldsymbol{h})$. □

In the following lemmas $\boldsymbol{q}$-restrictions are considered, with $\boldsymbol{q}\in\mathbb{Z}^3$. Here $\boldsymbol{q} = (q_1, q_2, q_3)$ is the coarsening factor, where usually $1 \le q_j \le 2$, $j = 1, 2, 3$.

Definition 4.8 Let $\boldsymbol{q}\in\mathbb{Z}^3$ with $\boldsymbol{q} > \mathbf{o}$ and $\boldsymbol{H} = \boldsymbol{qh}$, then the *canonical $\boldsymbol{q}$-restriction* $R^{\bullet}_{\boldsymbol{q}}$ is the operator $R^{\bullet}_{\boldsymbol{q}} : l(\mathbb{Z}_{\boldsymbol{h}}) \to l(\mathbb{Z}_{\boldsymbol{qh}}) = l(\mathbb{Z}_{\boldsymbol{H}})$, defined by

$$(R^{\bullet}_{\boldsymbol{q}} u^{\bullet}_{\boldsymbol{h}})(\boldsymbol{jH}) = u^{\bullet}_{\boldsymbol{H}}(\boldsymbol{jH}) = u^{\bullet}_{\boldsymbol{h}}(\boldsymbol{jqh})\,. \tag{61}$$

Theorem 4.9 We have the following relation between the FT of a grid function and that of its canonical $\boldsymbol{q}$-restriction,

$$\left(\widehat{R^{\bullet}_{\boldsymbol{q}} u^{\bullet}_{\boldsymbol{h}}}\right)(\boldsymbol{\omega}) = \sum_{\boldsymbol{p}\in[\mathbf{o},\boldsymbol{q})} \widehat{u^{\bullet}_{\boldsymbol{h}}}(\boldsymbol{\omega} + 2\pi\boldsymbol{p}/\boldsymbol{h}), \quad \forall\boldsymbol{\omega}\in T_{\boldsymbol{H}},\ \boldsymbol{H} = \boldsymbol{qh}. \tag{62}$$

Proof: The proof follows by a straightforward computation. □

Lemma 4.9 shows that, using the restriction $R^{\bullet}_{\boldsymbol{q}}$ with $\boldsymbol{q}\in\mathbb{Z}^3$, $\boldsymbol{q} > \mathbf{o}$, we get aliasing of $q^3 = q_1.q_2.q_3$ frequencies onto one.

Now we describe the relation between the Fourier transforms of a continuous function and its box restrictions. First we consider the direct restriction to the shifted grid, $R^{*}_{\boldsymbol{h}}$, and later the box-restriction, $R_{\boldsymbol{h}}$ and the $\boldsymbol{q}$-restriction $R^{*}_{\boldsymbol{q}}$.

Lemma 4.10

$$\widehat{u^{*}_{\boldsymbol{h}}}(\boldsymbol{\omega}) = \widehat{R^{*}_{\boldsymbol{h}} u}(\boldsymbol{\omega}) = \sum_{\boldsymbol{k}\in\mathbb{Z}^3} (-)^{|\boldsymbol{k}|} \hat{u}(\boldsymbol{\omega} + 2\pi\boldsymbol{k}/\boldsymbol{h})\,. \tag{63}$$

Proof:

$$\begin{aligned}
\widehat{u^\star_{\boldsymbol{h}}}(\boldsymbol{\omega}) &= \mathcal{F}(R^\star_{\boldsymbol{h}}u)(\boldsymbol{\omega}) = \left(\tfrac{h}{\sqrt{2\pi}}\right)^d \textstyle\sum_{\boldsymbol{j}} e^{-i(\boldsymbol{j}+\boldsymbol{e}/2)\boldsymbol{h}\boldsymbol{\omega}} u((\boldsymbol{j}+\boldsymbol{e}/2)\boldsymbol{h}) \\
&= \left(\tfrac{h}{\sqrt{2\pi}}\right)^d \textstyle\sum_{\boldsymbol{j}} e^{-i(\boldsymbol{j}+\boldsymbol{e}/2)\boldsymbol{h}\boldsymbol{\omega}} \left(\tfrac{1}{\sqrt{2\pi}}\right)^d \int e^{+i(\boldsymbol{j}+\boldsymbol{e}/2)\boldsymbol{h}\boldsymbol{z}}\, \widehat{u}(\boldsymbol{z})\, d\boldsymbol{z} \\
&= \left(\tfrac{h}{\sqrt{2\pi}}\right)^d \textstyle\sum_{\boldsymbol{j}} e^{-i(\boldsymbol{j}+\boldsymbol{e}/2)\boldsymbol{h}\boldsymbol{\omega}} \left(\tfrac{1}{\sqrt{2\pi}}\right)^d \\
&\quad \textstyle\sum_{\boldsymbol{k}} \int_{-\pi/\boldsymbol{h}}^{\pi/\boldsymbol{h}} e^{+i(\boldsymbol{j}+\boldsymbol{e}/2)\boldsymbol{h}(\boldsymbol{z}+2\pi\boldsymbol{k}/\boldsymbol{h})}\, \widehat{u}(\boldsymbol{z}+2\pi\boldsymbol{k}/\boldsymbol{h})\, d\boldsymbol{z} \\
&= \left(\tfrac{h}{2\pi}\right)^d \textstyle\sum_{\boldsymbol{j}} e^{-i(\boldsymbol{j}+\boldsymbol{e}/2)\boldsymbol{h}\boldsymbol{\omega}} \int_{-\pi/h}^{\pi/h} e^{+i(\boldsymbol{j}+\boldsymbol{e}/2)\boldsymbol{h}\boldsymbol{z}} \\
&\quad \textstyle\sum_{\boldsymbol{k}} (-)^{|\boldsymbol{k}|}\, \widehat{u}(\boldsymbol{z}+2\pi\boldsymbol{k}/\boldsymbol{h})\, d\boldsymbol{z}\,.
\end{aligned}$$

and using (56) and (57) we see

$$\widehat{u^\star_{\boldsymbol{h}}}(\boldsymbol{\omega}) = \widehat{R^\star_{\boldsymbol{h}}u}\,(\boldsymbol{\omega}) = \sum_{\boldsymbol{k}\in\mathbb{Z}^d} (-)^{|\boldsymbol{k}|}\, \widehat{u}(\boldsymbol{\omega}+2\pi\boldsymbol{k}/\boldsymbol{h})\,. \tag{64}$$

□

For the Fourier transform of $u \in L^2(\mathbb{R}^3)$ and $R_{\boldsymbol{h}}u \in L^2(\mathbb{R}^3)$ we have the following relation.

Theorem 4.11

$$\widehat{u_{\boldsymbol{h}}}(\boldsymbol{\omega}) = \widehat{R_{\boldsymbol{h}}u}(\boldsymbol{\omega}) = \sum_{\boldsymbol{k}\in\mathbb{Z}^3} (-)^{|\boldsymbol{k}|}\mathrm{Sinc}\,\Big(\frac{\boldsymbol{h}\boldsymbol{\omega}}{2\pi}+\boldsymbol{k}\Big)\cdot \widehat{u}(\boldsymbol{\omega}+2\pi\boldsymbol{k}/\boldsymbol{h})\,. \tag{65}$$

Proof: Using (53) we see

$$\begin{aligned}
\widehat{u^\star_{\boldsymbol{h}}}(\boldsymbol{\omega}) &= \mathcal{F}(R_{\boldsymbol{h}}u)(\boldsymbol{\omega}) = \left(\tfrac{2\pi}{h}\right)^{3/2} \mathcal{F}(R^\star_{\boldsymbol{h}}((D_{\boldsymbol{h}}\Pi)\star u))(\boldsymbol{\omega}) \\
&= \left(\tfrac{2\pi}{h}\right)^{3/2} \textstyle\sum_{\boldsymbol{k}} (-)^{|\boldsymbol{k}|}\, (\widehat{D_{\boldsymbol{h}}\Pi})(\boldsymbol{\omega}+2\pi\boldsymbol{k}/\boldsymbol{h})\cdot \widehat{u}(\boldsymbol{\omega}+2\pi\boldsymbol{k}/\boldsymbol{h}) \\
&= h^{-3/2} \textstyle\sum_{\boldsymbol{k}} (-)^{|\boldsymbol{k}|} D_{1/\boldsymbol{h}}\mathrm{Sinc}\,\big(\tfrac{\boldsymbol{\omega}}{2\pi}+\boldsymbol{k}/\boldsymbol{h}\big)\cdot \widehat{u}(\boldsymbol{\omega}+2\pi\boldsymbol{k}/\boldsymbol{h})\,. \\
&= \textstyle\sum_{\boldsymbol{k}} (-)^{|\boldsymbol{k}|}\mathrm{Sinc}\,\big(\tfrac{\boldsymbol{h}\boldsymbol{\omega}}{2\pi}+\boldsymbol{k}\big)\cdot \widehat{u}(\boldsymbol{\omega}+2\pi\boldsymbol{k}/\boldsymbol{h})\,.
\end{aligned} \tag{66}$$

□

Definition 4.12 Let $\boldsymbol{q}\in\mathbb{Z}^3$ with $\boldsymbol{q} > \mathbf{o}$ and $\boldsymbol{H} = \boldsymbol{q}\boldsymbol{h}$, then, for $\boldsymbol{s}\in[\mathbf{o},\boldsymbol{q})$, the *$\boldsymbol{s}$-frequency decomposition $\boldsymbol{q}$-restriction* is the operator $R^{\boldsymbol{s}}_{\boldsymbol{q}} : l(\mathbb{Z}_{\boldsymbol{h}}) \to l(\mathbb{Z}_{\boldsymbol{q}\boldsymbol{h}}) = l(\mathbb{Z}_{\boldsymbol{H}})$ is defined by

$$(R^{\boldsymbol{s}}_{\boldsymbol{q}}u^\star_{\boldsymbol{h}})((\boldsymbol{j}+\boldsymbol{e}/2)\boldsymbol{H}) = q^{-3}\textstyle\sum_{\boldsymbol{k}\in[\mathbf{o},\boldsymbol{q})}(-)^{\boldsymbol{s}\boldsymbol{k}}\, u^\star_{\boldsymbol{h}}((\boldsymbol{q}\boldsymbol{j}+\boldsymbol{k}+\boldsymbol{e}/2)\boldsymbol{h})\,, \tag{67}$$

where q^3 denotes $q^3 = q_1\cdot q_2\cdot q_3$.

Remarks:

- In the case $\boldsymbol{s} = \mathbf{o}$ we call $R^{\boldsymbol{s}}_{\boldsymbol{q}} = R^{\mathbf{o}}_{\boldsymbol{q}} = R^\star_{\boldsymbol{q}}$ simply the $\boldsymbol{q}$-restriction.
- From the construction of the restriction operators $R^B_{\boldsymbol{h}}$ and $R^\star_{\boldsymbol{q}}$ it is clear that the following relation holds:

$$R^B_{\boldsymbol{H}} = R^\star_{\boldsymbol{q}} R^B_{\boldsymbol{h}}\,.$$

Theorem 4.13 Let $\boldsymbol{q} = 2\boldsymbol{e} \in \mathbb{Z}^3$, then for all $\boldsymbol{\omega} \in T^3_{\boldsymbol{H}}$, $\boldsymbol{H} = 2\boldsymbol{h}$, we have

$$(\widehat{R^{\boldsymbol{s}}_{\boldsymbol{q}} u^\star_{\boldsymbol{h}}})(\boldsymbol{\omega}) = 2\, q^{-3} i^{\boldsymbol{s}} \sum_{\boldsymbol{m} \in [\mathbf{0},\boldsymbol{q})} (-)^{\boldsymbol{m}} \mathrm{Cos}\Big(\frac{\boldsymbol{h\omega} + \pi(\boldsymbol{m}+\boldsymbol{s})}{2}\Big) \cdot \widehat{u^\star_{\boldsymbol{h}}}(\boldsymbol{\omega} + \pi \boldsymbol{m}/\boldsymbol{h}) \qquad (68)$$

where

$$\mathrm{Cos}(\boldsymbol{h\omega}/2) = \prod_{j=1,2,3} \cos(h_j \omega_j/2)\,.$$

Proof: Using respectively the relations (54), (67) and (55) we have

$$\begin{aligned}
&(\widehat{R^{\boldsymbol{s}}_{\boldsymbol{q}} u^\star_{\boldsymbol{h}}})(\boldsymbol{\omega}) = (\tfrac{H}{\sqrt{2\pi}})^d \textstyle\sum_{\boldsymbol{j} \in \mathbb{Z}^d} e^{-i(\boldsymbol{j}+\boldsymbol{e}/2)\boldsymbol{H\omega}}\, u^\star_{\boldsymbol{H}}((\boldsymbol{j}+\boldsymbol{e}/2)\boldsymbol{H}) \\
= \;& \|\boldsymbol{q}\|^{-1} \textstyle\sum_{\boldsymbol{p},\boldsymbol{m} \in [\mathbf{0},\boldsymbol{q})} (-)^{\boldsymbol{sp}} e^{-i\boldsymbol{h\omega}} e^{+i(\boldsymbol{p}+\boldsymbol{e}/2)\boldsymbol{h}(\boldsymbol{\omega}+\pi\boldsymbol{m}/\boldsymbol{h})}\, \widehat{u^\star_{\boldsymbol{h}}}(\boldsymbol{\omega} + \pi\boldsymbol{m}/\boldsymbol{h}) \\
= \;& \|\boldsymbol{q}\|^{-1} (-i)^{\boldsymbol{s}} \textstyle\sum_{\boldsymbol{m} \in [\mathbf{0},\boldsymbol{q})} \frac{\mathrm{Sin}(\boldsymbol{h\omega})}{\mathrm{Sin}((\boldsymbol{h\omega}+\pi\boldsymbol{m}+\pi\boldsymbol{s})/2)} \cdot \widehat{u^\star_{\boldsymbol{h}}}(\boldsymbol{\omega} + \pi\boldsymbol{m}/\boldsymbol{h})\,,
\end{aligned}$$

where

$$\frac{\mathrm{Sin}(\boldsymbol{h\omega})}{\mathrm{Sin}((\boldsymbol{h\omega}+\pi\boldsymbol{m}+\pi\boldsymbol{s})/2)} = \prod_{j=1,\cdots,d} \frac{\sin h_j \omega}{\sin\,(\boldsymbol{h}_j\boldsymbol{\omega} + \pi \boldsymbol{m}_j + \pi \boldsymbol{s}_j)/2}\,.$$

With

$$\frac{\mathrm{Sin}(\boldsymbol{h\omega})}{\mathrm{Sin}((\boldsymbol{h\omega}+\pi\boldsymbol{m}+\pi\boldsymbol{s})/2)} = 2\,\mathrm{Cos}(\boldsymbol{h\omega}/2 - \pi(\boldsymbol{m}+\boldsymbol{s})/2)$$

we combine both equalities to obtain

$$\begin{aligned}
\widehat{u_{H+}}(\boldsymbol{\omega}) &= \|\boldsymbol{q}\|^{-1} (-i)^{|\boldsymbol{s}|} \textstyle\sum_{\boldsymbol{m} \in [\mathbf{0},\boldsymbol{q})} \frac{\mathrm{Sin}(\boldsymbol{h\omega})}{\mathrm{Sin}((\boldsymbol{h\omega}+\pi\boldsymbol{m}+\pi\boldsymbol{s})/2)}\, \widehat{u^\star_{\boldsymbol{h}}}(\boldsymbol{\omega} + \pi\boldsymbol{m}/\boldsymbol{h}) \\
&= 2\, \|\boldsymbol{q}\|^{-1} i^{|\boldsymbol{s}|} \textstyle\sum_{\boldsymbol{m} \in [\mathbf{0},\boldsymbol{q})} (-)^{\boldsymbol{m}} \mathrm{Cos}\big(\frac{\boldsymbol{h\omega}+\pi(\boldsymbol{m}+\boldsymbol{s})}{2}\big) \cdot \widehat{u^\star_{\boldsymbol{h}}}(\boldsymbol{\omega} + \pi\boldsymbol{m}/\boldsymbol{h})\,,
\end{aligned}$$

and

$$\begin{aligned}
&(\widehat{R^{\boldsymbol{s}}_{\boldsymbol{q}} u^\star_{\boldsymbol{h}}})(\boldsymbol{\omega}) = \\
&= (\tfrac{H}{\sqrt{2\pi}})^d \textstyle\sum_{\boldsymbol{j}}\; e^{-i(\boldsymbol{j}+\boldsymbol{e}/2)\boldsymbol{H\omega}} \|\boldsymbol{q}\|^{-1} \sum_{\boldsymbol{p} \in [\mathbf{0},\boldsymbol{q})} (-)^{\boldsymbol{sp}} u^\star_{\boldsymbol{h}}((\boldsymbol{qj}+\boldsymbol{p}+\boldsymbol{e}/2)\boldsymbol{h}) \\
&= \|\boldsymbol{q}\|^{-1} \textstyle\sum_{\boldsymbol{m} \in [\mathbf{0},\boldsymbol{q})} e^{i(\pi\boldsymbol{m}-\boldsymbol{h\omega})/2} \sum_{\boldsymbol{p} \in [\mathbf{0},\boldsymbol{q})} e^{i\boldsymbol{p}(\boldsymbol{h\omega}+\pi\boldsymbol{m}+\pi\boldsymbol{s})} \cdot \widehat{u^\star_{\boldsymbol{h}}}(\boldsymbol{\omega} + \pi\boldsymbol{m}/\boldsymbol{h}) \\
&= \|\boldsymbol{q}\|^{-1} \textstyle\sum_{\boldsymbol{m} \in [\mathbf{0},\boldsymbol{q})} e^{+i(\pi\boldsymbol{m}-\boldsymbol{h\omega})/2} \cdot \prod_{j=1}^d \frac{1-e^{+i2h_j\boldsymbol{\omega}}}{1-e^{+i(h_j\boldsymbol{\omega}+\pi\boldsymbol{m}_j+\pi\boldsymbol{s}_j)}} \cdot \widehat{u^\star_{\boldsymbol{h}}}(\boldsymbol{\omega} + \pi\boldsymbol{m}/\boldsymbol{h}) \\
&= \|\boldsymbol{q}\|^{-1} (-i)^{\boldsymbol{s}} \textstyle\sum_{\boldsymbol{m} \in [\mathbf{0},\boldsymbol{q})} \frac{\mathrm{Sin}(\boldsymbol{h\omega})}{\mathrm{Sin}((\boldsymbol{h\omega}+\pi\boldsymbol{m}+\pi\boldsymbol{s})/2)} \cdot \widehat{u^\star_{\boldsymbol{h}}}(\boldsymbol{\omega} + \pi\boldsymbol{m}/\boldsymbol{h})\,,
\end{aligned}$$

where

$$\frac{\mathrm{Sin}(\boldsymbol{h\omega})}{\mathrm{Sin}((\boldsymbol{h\omega}+\pi\boldsymbol{m}+\pi\boldsymbol{s})/2)} = \textstyle\prod_{j=1,\cdots,d} \frac{\sin h_j\omega}{\sin\,(h_j\boldsymbol{\omega}+\pi m_j+\pi\boldsymbol{\omega})/2}\,,$$

with

$$\frac{\mathrm{Sin}(\boldsymbol{h\omega})}{\mathrm{Sin}((\boldsymbol{h\omega}+\pi\boldsymbol{m}+\pi\boldsymbol{s})/2)} = 2\,\mathrm{Cos}(\boldsymbol{h\omega}/2 - \pi(\boldsymbol{m}+\boldsymbol{s})/2)\,. \qquad (69)$$

We combine both equalities to obtain

$$\begin{aligned}
\widehat{u^\star_{\boldsymbol{H}}}(\boldsymbol{\omega}) &= \|\boldsymbol{q}\|^{-1} (-i)^{|\boldsymbol{s}|} \textstyle\sum_{\boldsymbol{m} \in [\mathbf{0},\boldsymbol{q})} \frac{\mathrm{Sin}(\boldsymbol{h\omega})}{\mathrm{Sin}((\boldsymbol{h\omega}+\pi\boldsymbol{m}+\pi\boldsymbol{s})/2)}\, \widehat{u^\star_{\boldsymbol{h}}}(\boldsymbol{\omega} + \pi\boldsymbol{m}/\boldsymbol{h}) \\
&= 2\, \|\boldsymbol{q}\|^{-1} i^{|\boldsymbol{s}|} \textstyle\sum_{\boldsymbol{m} \in [\mathbf{0},\boldsymbol{q})} (-)^{\boldsymbol{m}} \mathrm{Cos}\big(\frac{\boldsymbol{h\omega}+\pi(\boldsymbol{m}+\boldsymbol{s})}{2}\big) \cdot \widehat{u^\star_{\boldsymbol{h}}}(\boldsymbol{\omega} + \pi\boldsymbol{m}/\boldsymbol{h})\,.
\end{aligned}$$

□

Definition 4.14 The *natural box-prolongation* $P_{\boldsymbol{h}}^{\star} : l^2(\mathbb{Z}_{\boldsymbol{h}}^{\star}) \rightarrow L^2(\mathbb{R}^3)$ is defined by

$$u(\boldsymbol{x}) = (P_{\boldsymbol{h}}^{\star} u_{\boldsymbol{h}}^{\star})(\boldsymbol{x}) = u_{\boldsymbol{h}}((\boldsymbol{m} + \boldsymbol{e}/2)\boldsymbol{h}),$$

for all $\boldsymbol{m} \in \mathbb{Z}^3$ and $\boldsymbol{mh} < \boldsymbol{x} < (\boldsymbol{m} + \boldsymbol{e})\boldsymbol{h}$. We also introduce a *natural prolongation*, $P_{\boldsymbol{q}}^{\star}$, from a coarse to a fine gridfunction $P_{\boldsymbol{q}}^{\star} : l^2(\mathbb{Z}_{\boldsymbol{H}}^{\star}) \rightarrow l^2(\mathbb{Z}_{\boldsymbol{h}}^{\star})$ by $P_{\boldsymbol{q}}^{\star} = R_{\boldsymbol{h}}^{\star} P_{\boldsymbol{H}}^{\star}$ where $\boldsymbol{H} = \boldsymbol{qh}$. The *prolongation* $P_{\boldsymbol{h}}^{B} : l(\mathbb{Z}_{\boldsymbol{h}}^{\star}) \rightarrow L^2(\mathbb{R}^3)$ is the operator dual to $R_{\boldsymbol{h}}^{B}$ in the sense that for all $u_{\boldsymbol{h}}^{\star} \in l^2(\mathbb{Z}_{\boldsymbol{h}}^{\star})$ and $v \in L^2(\mathbb{R}^3)$ we have

$$< P_{\boldsymbol{h}}^{B} u_{\boldsymbol{h}}^{\star}, v >_{L^2(\mathbb{R}^3)} = < u_{\boldsymbol{h}}^{\star}, R_{\boldsymbol{h}}^{B} v >_{l^2(\mathbb{Z}_{\boldsymbol{h}}^{\star})} . \tag{70}$$

The following theorems show how we find the FT of the prolongation if the FT of the source function is given.

Lemma 4.15

$$\widehat{u}(\boldsymbol{\omega}) = \mathcal{F}(P_{\boldsymbol{h}}^{\star} u_{\boldsymbol{h}}^{\star})(\boldsymbol{\omega}) = \frac{\mathrm{Sin}(\boldsymbol{h\omega}/2)}{\boldsymbol{h\omega}/2} \widehat{u_{\boldsymbol{h}}^{\star}}(\boldsymbol{\omega}) . \tag{71}$$

Proof:

$$\begin{aligned}
\widehat{u}(\boldsymbol{\omega}) &= (2\pi)^{-d/2} \textstyle\int_{\mathbb{R}^d} e^{-i\boldsymbol{x\omega}} u(\boldsymbol{x})\, d\boldsymbol{x} \quad (\text{with } \boldsymbol{x} = \boldsymbol{mh} + \xi h, 0 \leq \xi < 1) \\
&= (2\pi)^{-d/2} \textstyle\sum_{m \in \mathbb{Z}^d} \int_{\xi \in [0,1)^d} e^{-i(\boldsymbol{m}+\xi)\boldsymbol{\omega h}} u((\boldsymbol{m} + \xi)\boldsymbol{h})\, d(\xi \boldsymbol{h}) \\
&= \widehat{u_{\boldsymbol{h}}^{\star}}(\boldsymbol{\omega}) \textstyle\int_{\xi \in [0,1)^d} e^{-i(\xi - \boldsymbol{e}/2)\boldsymbol{\omega h}}\, d\xi \\
&= \widehat{u_{\boldsymbol{h}}^{\star}}(\boldsymbol{\omega}) \frac{1}{-i\boldsymbol{\omega h}} e^{-i\xi\boldsymbol{\omega h}} \Big|_{-1/2}^{+1/2} \\
&= \widehat{u_{\boldsymbol{h}}^{\star}}(\boldsymbol{\omega}) \frac{2}{\boldsymbol{\omega h}} \mathrm{Sin}(\boldsymbol{\omega h}/2) .
\end{aligned} \tag{72}$$

□

Theorem 4.16 With $\boldsymbol{H} = \boldsymbol{qh}$ and $q^3 = q_1.q_2.q_3$, we have for the FT of the prolongation of a box gridfunction

$$\widehat{u_{\boldsymbol{h}}^{\star}}(\boldsymbol{\omega}) = \mathcal{F}(P_{\boldsymbol{q}}^{\star} u_{\boldsymbol{H}}^{\star})(\boldsymbol{\omega}) = q^{-3} \frac{\mathrm{Sin}(\boldsymbol{H\omega}/2)}{\mathrm{Sin}(\boldsymbol{h\omega}/2)} \widehat{u_{\boldsymbol{H}}^{\star}}(\boldsymbol{\omega}) . \tag{73}$$

Proof:

$$\begin{aligned}
\widehat{u_{\boldsymbol{h}}^{\star}}(\boldsymbol{\omega}) &= \left(\tfrac{h}{\sqrt{2\pi}}\right)^d \textstyle\sum_{j \in \mathbb{Z}^d} e^{-i(j+\boldsymbol{e}/2)\boldsymbol{h\omega}} u_{\boldsymbol{h}}^{\star}((j + \boldsymbol{e}/2)\boldsymbol{h}) \\
&= \|\boldsymbol{q}\|^{-1} \widehat{u_{\boldsymbol{H}}^{\star}}(\boldsymbol{\omega}) \frac{e^{iH\boldsymbol{\omega}/2} - e^{-iH\boldsymbol{\omega}/2}}{e^{ih\boldsymbol{\omega}/2} - e^{-ih\boldsymbol{\omega}/2}} = \widehat{u_{\boldsymbol{H}}^{\star}}(\boldsymbol{\omega})\, \|\boldsymbol{q}\|^{-1} \frac{\mathrm{Sin}(\boldsymbol{\omega} H/2)}{\mathrm{Sin}(\boldsymbol{\omega} h/2)} .
\end{aligned} \tag{74}$$

□

THE FOURIER TRANSFORM OF OPERATORS INVOLVING DIFFERENT GRIDS.
In (68) and (73) we see that, by the restriction and prolongation between functions on grids $\Omega_{\boldsymbol{n}}$ and $\Omega_{\boldsymbol{n}+\boldsymbol{q}}$, aliasing takes place and that q^3 frequencies on $\Omega_{\boldsymbol{n}+\boldsymbol{q}}$ correspond with a single frequency on $\Omega_{\boldsymbol{n}}$. This implies that, analysing a multigrid algorithm, we have to study the behaviour of the q^3 aliasing frequencies together. Collecting the q^3 corresponding amplitudes of the aliasing frequencies in a single q^3-vector, we extend the definition (58) of $\mathcal{F}$ to the case $q^3 > 1$ and obtain $\mathcal{F} : l^2(\mathbb{Z}_{\boldsymbol{h}}) \rightarrow [L^2(T_{\boldsymbol{qh}})]^{q^3}$ or $\mathcal{F} : l^2(\mathbb{Z}_{\boldsymbol{h}}^{\star}) \rightarrow [L^2(T_{\boldsymbol{qh}})]^{q^3}$ by

$$\mathcal{F}(u_{\boldsymbol{h}})(\boldsymbol{\omega}) = \left(\widehat{u}_{\boldsymbol{h}}(\boldsymbol{\omega} + \pi \boldsymbol{m}/\boldsymbol{h})\right)_{\boldsymbol{m} \in [\boldsymbol{0},\boldsymbol{q})} , \quad \boldsymbol{\omega} \in T_{\boldsymbol{qh}} . \tag{75}$$

With these amplitude-vectors $\mathcal{F}(u_{\boldsymbol{h}}^{\bullet})(\boldsymbol{\omega})$ and $\mathcal{F}(u_{\boldsymbol{h}}^{\star})(\boldsymbol{\omega})$, we can introduce the linear operators $\mathcal{F}(R_{\boldsymbol{q}}^{\bullet})(\boldsymbol{\omega})$ and $\mathcal{F}(R_{\boldsymbol{q}}^{\star})(\boldsymbol{\omega})$ by

$$\mathcal{F}(R_{\boldsymbol{q}}^{\bullet}u_{\boldsymbol{h}}^{\bullet})(\boldsymbol{\omega}) = \mathcal{F}(R_{\boldsymbol{q}}^{\bullet})(\boldsymbol{\omega})\ \mathcal{F}(u_{\boldsymbol{h}}^{\bullet})(\boldsymbol{\omega})\ , \quad \boldsymbol{\omega}\in T_{\boldsymbol{qh}}\ , \tag{76}$$

and

$$\mathcal{F}(R_{\boldsymbol{q}}^{\star}u_{\boldsymbol{h}}^{\star})(\boldsymbol{\omega}) = \mathcal{F}(R_{\boldsymbol{q}}^{\star})(\boldsymbol{\omega})\ \mathcal{F}(u_{\boldsymbol{h}}^{\star})(\boldsymbol{\omega})\ , \quad \boldsymbol{\omega}\in T_{\boldsymbol{qh}}\ . \tag{77}$$

We call the new operators, that depend on $\boldsymbol{\omega}$, the Fourier transforms of the original operators. The new operators are $\ell \times q^3\ell$ matrices if ℓ aliasing frequencies are considered on the coarse grid.

Similar to the restrictions, the prolongations can be associated with their Fourier transforms.

$$\mathcal{F}(P_{\boldsymbol{q}}^{\bullet}u_{\boldsymbol{h}}^{\bullet})(\boldsymbol{\omega}) = \mathcal{F}(P_{\boldsymbol{q}}^{\bullet})(\boldsymbol{\omega})\ \mathcal{F}(u_{\boldsymbol{h}}^{\bullet})(\boldsymbol{\omega})\ , \quad \boldsymbol{\omega}\in T_{\boldsymbol{qh}}\ , \tag{78}$$

and

$$\mathcal{F}(P_{\boldsymbol{q}}^{\star}u_{\boldsymbol{h}}^{\star})(\boldsymbol{\omega}) = \mathcal{F}(P_{\boldsymbol{q}}^{\star})(\boldsymbol{\omega})\ \mathcal{F}(u_{\boldsymbol{h}}^{\star})(\boldsymbol{\omega})\ , \quad \boldsymbol{\omega}\in T_{\boldsymbol{qh}}\ . \tag{79}$$

These operators are $q^3\ell \times \ell$ matrices.

For arbitrary linear constant coefficient operators $A_{\boldsymbol{h}} : l^2(\mathbb{Z}_{\boldsymbol{h}}) \rightarrow l^2(\mathbb{Z}_{\boldsymbol{h}})$, its Fourier transform $\mathcal{F}(A_{\boldsymbol{h}}) : L^2(T_{\boldsymbol{h}}) \rightarrow L^2(T_{\boldsymbol{h}})$, can also be considered as a $q^3\ell \times q^3\ell$ diagonal matrix

$$\mathcal{F}(A_{\boldsymbol{h}}u_{\boldsymbol{h}})(\boldsymbol{\omega}) = \mathcal{F}(A_{\boldsymbol{h}})(\boldsymbol{\omega})\ \cdot\ \mathcal{F}(u_{\boldsymbol{h}})(\boldsymbol{\omega}) \qquad \forall \boldsymbol{\omega}\in T_{\boldsymbol{qh}}\ .$$

Because of Parseval's equality we know that

$$\|A_{\boldsymbol{h}}\|_2 = \max_{\boldsymbol{\omega}\in T_{\boldsymbol{qh}}} \|\ \mathcal{F}(A_{\boldsymbol{h}})(\boldsymbol{\omega})\|_2 = \max_{\boldsymbol{\omega}\in T_{\boldsymbol{qh}}} \sigma(\ \mathcal{F}(A_{\boldsymbol{h}})\ )\ (\boldsymbol{\omega})\,, \tag{80}$$

with $\sigma(A)$ the spectral norm (the largest singular value) of the matrix A, and

$$\rho(A_{\boldsymbol{h}}) = \max_{\boldsymbol{\omega}\in T_{\boldsymbol{qh}}} \rho(\ \mathcal{F}(A_{\boldsymbol{h}})\ )\ (\boldsymbol{\omega})\,, \tag{81}$$

where ρ denotes the spectral radius. This provides us with the means to study the norm and the spectral radius of the error-amplification operator of the multigrid iteration.

4.2 Convergence analysis results

To get some insight in the behaviour of the more-dimensional multigrid algorithm introduced in Section 3, we use Fourier analysis to determine the convergence rate of the two-level algorithm for the two-dimensional anisotropic Poisson equation

$$u_{xx} + \varepsilon^2 u_{yy} = f\,, \tag{82}$$

discretised by the usual 5-point discretisation.

The error-amplification operator, $M_{\boldsymbol{n}}$, of the two-level cycle (with μ pre- and ν post-relaxation steps) for the solution of (28) is described by

$$e_{\boldsymbol{n}}^{(i+1)} = M_{\boldsymbol{n}}\ e_{\boldsymbol{n}}^{(i)} = S_{\boldsymbol{n}}^{\nu}\ C_{\boldsymbol{n}}\ S_{\boldsymbol{n}}^{\mu}\ e_{\boldsymbol{n}}^{(i)}\ , \tag{83}$$

where $S_{\boldsymbol{n}}$ denotes the smoothing, e.g. damped Jacobi iteration:

$$e_{\boldsymbol{n}}^{(\text{new})} = S_{\boldsymbol{n}} e_{\boldsymbol{n}}^{(\text{old})} = \left(I_{\boldsymbol{n}} - \alpha D_{\boldsymbol{n}}^{-1} L_{\boldsymbol{n}}\right) e_{\boldsymbol{n}}^{(\text{old})}\ , \tag{84}$$

with α the damping parameter and $D_{\boldsymbol{n}}$ the main diagonal of the discrete operator $L_{\boldsymbol{n}}$. The coarse grid correction is described by (29) and (30). For gridfunctions $u_{\boldsymbol{h}} \in l^2(\mathbb{Z}^{\star}_{\boldsymbol{h}})$, i.e. neglecting boundary conditions, we find, using (29)

$$\mathcal{F}(M_{\boldsymbol{n}})(\boldsymbol{\omega}) = \mathcal{F}(S_{\boldsymbol{n}})^{\nu}(\boldsymbol{\omega}) \;\; \mathcal{F}(C_{\boldsymbol{n}})(\boldsymbol{\omega}) \;\; \mathcal{F}(S_{\boldsymbol{n}})^{\mu}(\boldsymbol{\omega}) \,, \tag{85}$$

with

$$\mathcal{F}(S_{\boldsymbol{n}}) = \mathcal{F}(I_{\boldsymbol{n}}) - \alpha \; \mathcal{F}(D_{\boldsymbol{n}})^{-1} \; \mathcal{F}(L_{\boldsymbol{n}}) \,, \tag{86}$$

and

$$\begin{aligned} \mathcal{F}(C_{\boldsymbol{n}}) \;=\; & \mathcal{F}(I_{\boldsymbol{n}}) \\ & - \sum_{j=1,2,3} \mathcal{F}(P_{\boldsymbol{n},\boldsymbol{n}-\boldsymbol{e}_j}) \; \mathcal{F}(L_{\boldsymbol{n}-\boldsymbol{e}_j})^{-1} \; \mathcal{F}(R_{\boldsymbol{n}-\boldsymbol{e}_j,\boldsymbol{n}}) \; \mathcal{F}(L_{\boldsymbol{n}}) \\ & + \sum_{j=1,2,3} \mathcal{F}(P_{\boldsymbol{n},\boldsymbol{n}-\boldsymbol{e}+\boldsymbol{e}_j}) \; \mathcal{F}(L_{\boldsymbol{n}-\boldsymbol{e}+\boldsymbol{e}_j})^{-1} \; \mathcal{F}(R_{\boldsymbol{n}-\boldsymbol{e}+\boldsymbol{e}_j,\boldsymbol{n}}) \; \mathcal{F}(L_{\boldsymbol{n}}) \\ & - \mathcal{F}(P_{\boldsymbol{n},\boldsymbol{n}-\boldsymbol{e}}) \; \mathcal{F}(L_{\boldsymbol{n}-\boldsymbol{e}})^{-1} \; \mathcal{F}(R_{\boldsymbol{n}-\boldsymbol{e},\boldsymbol{n}}) \; \mathcal{F}(L_{\boldsymbol{n}}) \,. \end{aligned} \tag{87}$$

To get an impression of the behaviour of the algorithm, keeping the explicit computation to reasonable size, we elaborate (85) for the equation (82), for the two-dimensional case, with $\boldsymbol{q} = (2,2)$ and $\mu = \nu = 1$. Then $\mathcal{F}(M_{\boldsymbol{n}})(\boldsymbol{\omega})$ is a 4×4-matrix, which we derive from (85), (86) and (cf. (13))

$$\begin{aligned} \mathcal{F}(C_{\boldsymbol{n}}) \;=\; & \mathcal{F}(I_{\boldsymbol{n}}) \\ & - \mathcal{F}(P_{\boldsymbol{n},\boldsymbol{n}-\boldsymbol{e}_1}) \; \mathcal{F}(L_{\boldsymbol{n}-\boldsymbol{e}_1})^{-1} \; \mathcal{F}(R_{\boldsymbol{n}-\boldsymbol{e}_1,\boldsymbol{n}}) \; \mathcal{F}(L_{\boldsymbol{n}}) \\ & - \mathcal{F}(P_{\boldsymbol{n},\boldsymbol{n}-\boldsymbol{e}_2}) \; \mathcal{F}(L_{\boldsymbol{n}-\boldsymbol{e}_2})^{-1} \; \mathcal{F}(R_{\boldsymbol{n}-\boldsymbol{e}_2,\boldsymbol{n}}) \; \mathcal{F}(L_{\boldsymbol{n}}) \\ & + \mathcal{F}(P_{\boldsymbol{n},\boldsymbol{n}-\boldsymbol{e}}) \; \mathcal{F}(L_{\boldsymbol{n}-\boldsymbol{e}})^{-1} \; \mathcal{F}(R_{\boldsymbol{n}-\boldsymbol{e},\boldsymbol{n}}) \; \mathcal{F}(L_{\boldsymbol{n}}) \,. \end{aligned}$$

From (68) and (73) we know

$$\mathcal{F}(R_{\boldsymbol{n}-\boldsymbol{e}_1,\boldsymbol{n}}) = \begin{pmatrix} \cos\omega_2 h_2 & 0 & \sin\omega_2 h_2 & 0 \\ 0 & \cos\omega_2 h_2 & 0 & \sin\omega_2 h_2 \end{pmatrix} ,$$

$$\mathcal{F}(R_{\boldsymbol{n}-\boldsymbol{e}_2,\boldsymbol{n}}) = \begin{pmatrix} \cos\omega_1 h_1 & \sin\omega_1 h_1 & 0 & 0 \\ 0 & 0 & \cos\omega_1 h_1 & \sin\omega_1 h_1 \end{pmatrix}$$

and

$$\mathcal{F}(R_{\boldsymbol{n}-\boldsymbol{e},\boldsymbol{n}}) = \begin{pmatrix} \cos(\omega_1 h_1)\cos(\omega_2 h_2) \\ \sin(\omega_1 h_1)\cos(\omega_2 h_2) \\ \cos(\omega_1 h_1)\sin(\omega_2 h_2) \\ \sin(\omega_1 h_1)\sin(\omega_2 h_2) \end{pmatrix}^T .$$

So that with $\mathcal{F}(P_{\boldsymbol{n},\boldsymbol{n}-\boldsymbol{e}_1}) = \mathcal{F}(R_{\boldsymbol{n}-\boldsymbol{e}_1,\boldsymbol{n}})^T$, $\mathcal{F}(P_{\boldsymbol{n},\boldsymbol{n}-\boldsymbol{e}_2}) = \mathcal{F}(R_{\boldsymbol{n}-\boldsymbol{e}_2,\boldsymbol{n}})^T$ and $\mathcal{F}(P_{\boldsymbol{n},\boldsymbol{n}-\boldsymbol{e}}) = \mathcal{F}(R_{\boldsymbol{n}-\boldsymbol{e},\boldsymbol{n}})^T$, the norm $\|M_{\boldsymbol{n}}\|$ and the spectral radius $\rho(M_{\boldsymbol{n}})$ can be computed by means of (80) and (81).

To study the convergence behaviour of our algorithm, we consider the matrices (86), (87) and (85) as a function of $\boldsymbol{\omega} \in T_{\boldsymbol{h}} = [-\pi/h, \pi/h]^2$, and for each $\boldsymbol{\omega}$ we compute its eigenvalues and singular values of these matrices. We show these values in Fig. 1 for the case $\alpha = 2/3$, $\varepsilon = 1$. Without loss of generality we can take $\boldsymbol{h} = (1,1)$, the parameter ε taking care of the anisotropy. The damping parameter $\alpha \in [0,1]$ for the Jacobi relaxation, can be chosen freely. We select the value $\alpha = 2/3$ because it minimises

$$\max_{\boldsymbol{\omega}=(0,\pi/h),(\phi,0),(\pi/h,\pi/h)} \rho(\; \mathcal{F}(S_{\boldsymbol{n}})(\boldsymbol{\omega})) \,.$$

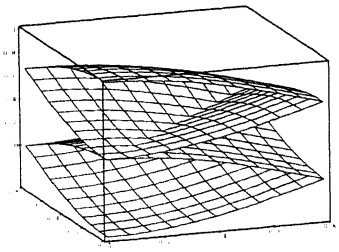

a. The eigenvalues of $\mathcal{F}(S_{\boldsymbol{n}})(\omega)$.

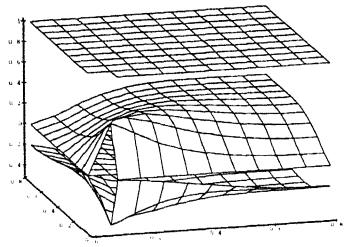

b. The eigenvalues of $\mathcal{F}(C_{\boldsymbol{n}})(\omega)$.

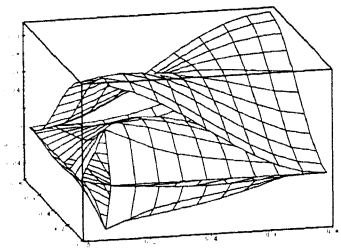

(c) The eigenvalues of $\mathcal{F}(M_{\boldsymbol{n}})(\omega)$.

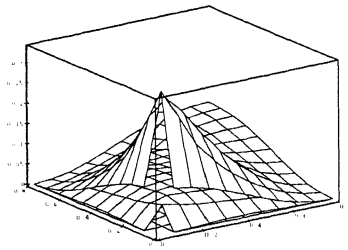

(d) The singular values of $\mathcal{F}(M_{\boldsymbol{n}})(\omega)$.

Figure 1: The frequency response of the smoothing, CGC and TLA operators for $\varepsilon = 1$, $\boldsymbol{q} = (2,2)$ and $\alpha = 2/3$.

This means that $\alpha = 2/3$ makes $S_{\boldsymbol{n}}$ a well balanced smoother for the different types of high frequencies (see Fig. 1.a).

In Fig. 1.a we show the eigenvalues of the smoothing operator, and in Fig. 1.b of the coarse grid correction. In this figure we see that one eigenvalue of $\mathcal{F}(C_{\boldsymbol{n}})$ is always equal to one. This eigenvalue corresponds with the highest frequencies, for which no correction can be obtained from any of the three coarser grids. The combined effect of the smoother and the coarse grid correction is seen in Fig. 1.c, which shows that $\sup_{\boldsymbol{\omega}} \rho(M_{\boldsymbol{n}}(\omega)) \approx 1/9$, and also in Fig. 1.d, where we see $\sup_{\boldsymbol{\omega}} \|M_{\boldsymbol{n}}(\omega)\| \approx 1/3$. The rather low maximal values show that -at least for square fine-grid cells- the multigrid algorithm has good convergence behaviour.

Because it is important that the algorithm is effective for an arbitrary cell aspect ratio, in the Figs 2 - 4 we show the singular values of $\mathcal{F}(M_{\boldsymbol{n}})(\omega)$ also for $\varepsilon = 1/8$ and for the limit as $\varepsilon \to 0$. Now it appears that for high aspect ratios the convergence behaviour deteriorates. We find $\sup_{\boldsymbol{\omega}} \lim_{\varepsilon \to 0} \sigma(\ \mathcal{F}(M_{\boldsymbol{n}})(\omega)) \approx 5$. This implies that we cannot always guarantee error reduction for a single iteration sweep. Therefore we show in Fig. 4 also the behaviour of $M^2_{\boldsymbol{n}}(\omega)$. This shows that a couple of two consecutive iteration steps does guarantee error reduction, and the convergence rate is significant:

$$\sup_{\boldsymbol{\omega}} \lim_{\varepsilon \to 0} \rho(\ \mathcal{F}(M^2_{\boldsymbol{n}})(\omega)) \approx 1/9 \ .$$

As a consequence we can expect that a W-type cycle of the multigrid algorithm will have good convergence properties.

From the computations of which the results are summarised in the Figs 2 - 4, we conclude that the eigenvalues of the iteration matrix are less that 1, uniformly in the

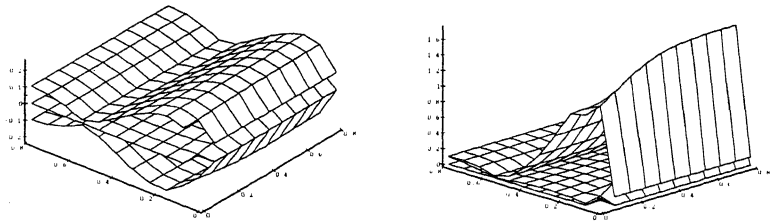

a. The eigenvalues of $\mathcal{F}(M_{\boldsymbol{n}})(\boldsymbol{\omega})$. b. The singular values of $\mathcal{F}(M_{\boldsymbol{n}})(\boldsymbol{\omega})$.

Figure 2: The frequency response of the TLA operator $M_{\boldsymbol{n}}$ for $\varepsilon = 1/8$, $\boldsymbol{q} = (2, 2)$ and $\alpha = 2/3$.

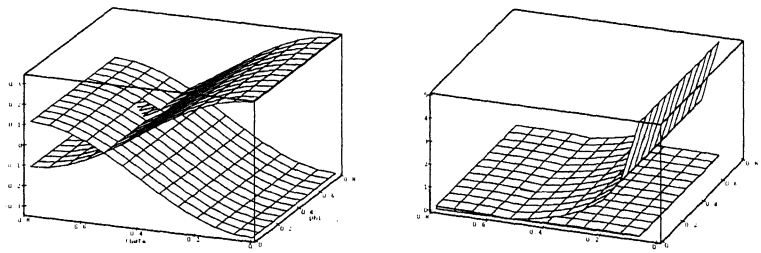

a. The eigenvalues of $\lim_{\varepsilon \to 0} \mathcal{F}(M_{\boldsymbol{n}})(\boldsymbol{\omega})$.

b. The singular values of $\lim_{\varepsilon \to 0} \mathcal{F}(M_{\boldsymbol{n}})(\boldsymbol{\omega})$.

Figure 3: The frequency response of the TLA operator for $\lim_{\varepsilon \to 0} M_{\boldsymbol{n}}$, for $\boldsymbol{q} = (2, 2)$ and $\alpha = 2/3$.

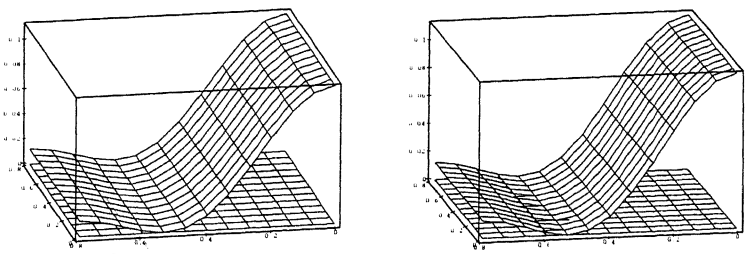

a. The eigenvalues of $\lim_{\varepsilon \to 0} \mathcal{F}(M_{\boldsymbol{n}}^2)(\boldsymbol{\omega})$.

b. The singular values of $\lim_{\varepsilon \to 0} \mathcal{F}(M_{\boldsymbol{n}}^2)(\boldsymbol{\omega})$.

Figure 4: The frequency response of the TLA operator $\lim_{\varepsilon \to 0} M_{\boldsymbol{n}}^2$, for $\boldsymbol{q} = (2, 2)$ and $\alpha = 2/3$.

parameter ε. In fact, $\max_\varepsilon \rho(M_{\boldsymbol{n}}) \approx 0.33$ and $\max_\varepsilon \|M_{\boldsymbol{n}}\| \approx 5.0$ and $\max_\varepsilon \|M_{\boldsymbol{n}}^2\| \approx 0.11$. The fact that $\|M_{\boldsymbol{n}}\| > 1$ and $\|M_{\boldsymbol{n}}^2\| << 1$ shows that, in general, a W-cycle will be necessary to guarantee a good convergence rate for the algorithm.

Although only 4×4-matrices, the expressions for $\mathcal{F}(M_{\boldsymbol{n}})(\boldsymbol{\omega})$ or $\mathcal{F}(C_{\boldsymbol{n}})(\boldsymbol{\omega})$ are too complex to show them here explicitly. However, to understand their behaviour it is interesting, however, to see how the matrices behave in the neighbourhood of the origin. Therefore we expand the elements of $\mathcal{F}(M_{\boldsymbol{n}})(\boldsymbol{\omega})$ in powers of ω and we show the principal terms. We see that for $\mathcal{F}(M_{\boldsymbol{n}})(\omega)$ a singularity exists at the origin. The limit $\lim_{\omega \to 0} \mathcal{F}(M_{\boldsymbol{n}})(\boldsymbol{\omega})$ depends on the ratio $\sigma = \omega_2/\omega_1$. This is the reason why the eigen- and singular values are missing at $\boldsymbol{\omega} = \mathbf{o}$ in the Figs 1 and 2.

5 Conclusion

We introduced a multigrid algorithm for second order elliptic equations in three dimensions, discretised by a finite-volume method. For the approximation we use piecewise constant basis functions, that are the tensor product generalisation of the one-dimensional case. Using a family of uniform grids, each with a different mesh size in a different coordinate direction, we obtain a hierarchy of approximations. The corresponding set of function spaces can be interpreted in terms of wavelet terminology as a three-dimensional multiresolution analysis. Following the idea of sparse grids, a selection of degrees of freedom is made, that gives a high accuracy for a relatively small number of degrees of freedom, provided that a certain smoothness requirement is satisfied.

A multigrid algorithm of additive Schwarz type is constructed for the solution of the discrete system, and its convergence is analysed by Fourier analysis. For this purpose the necessary tools are developed for the Fourier analysis of box-grid functions.

From the analysis we conclude that, with simple damped Jacobi iteration as a smoother, the spectral radius of the multigrid iteration matrix is less that 1, uniformly in the cell aspect ratio.

The spectral norm can be larger that one. We find $\max_\varepsilon \|M_{\boldsymbol{n}}\| \approx 5.0$. This may indicate that a V-cycle type algorithm will not converge. However, it appears that $\max_\varepsilon \|M_{\boldsymbol{n}}^2\| \approx 0.11$. This shows that, in general, a W-cycle will be necessary to guarantee a good convergence rate for the algorithm. Independent of the cell aspect ratio, we find the spectral radius $\rho(M_{\boldsymbol{n}}) \leq 0.33$.

References

[1] R. N. Bracewell. *The Fourier Transform and its Applications.* McGraw-Hill International Eds, 1986.

[2] I. Daubechies. *Ten Lectures on Wavelets*, volume 61 of *CBMS-NSF regional conference series in applied mathematics.* SIAM, 1992.

[3] M. Griebel, M. Schneider, and C. Zenger. A combination technique for the solution of sparse grid problems. Technical Report TUM-I 9038, SFB 342/19/90A, TU München, 1990.

[4] P.W. Hemker. Sparse-Grid Finite-Volume Multigrid for 3D-Problems, *Advances in Comput. Math.*, 4, 83–110 (1995).

[5] P.W. Hemker and P.M. de Zeeuw. BASIS3: A data structure for 3-dimensional sparse grids. This volume.

[6] W. Mulder. A high-resolution Euler solver based on multigrid semi-coarsening, and defect correction. *Journal of Computational Physics*, 100:91–104, 1992.

[7] W.A. Mulder. A new multigrid approach to convection problems. *Journal of Computational Physics*, pages 303–323, 1989.

[8] N.H. Naik and J. Van Rosendale. The improved robustness of multigrid elliptic solvers based on multiple semicoarsened grids. Technical Report No. 91-70, ICASE, 1991.

[9] C. Zenger. Sparse grids. In W. Hackbusch, editor, *Parallel Algorithms for PDE, Proc. 6th GAMM Seminar, Kiel 1990*, pages 241–251, Braunschweig, 1991. Vieweg.